

ICONS: Influence Consensus for Vision-Language Data Selection

Xindi Wu¹Mengzhou Xia¹
Pang Wei Koh^{2,4}¹Princeton University²University of WashingtonRulin Shao²
Olga Russakovsky¹Zhiwei Deng³
Allen Institute for AI³Google DeepMind

<https://princetonvisualai.github.io/icons/>

Abstract

Training vision-language models via instruction tuning relies on large data mixtures spanning diverse tasks and domains, yet these mixtures frequently include redundant information that increases computational costs without proportional gains. Existing methods typically rely on task-agnostic heuristics to estimate data importance, limiting their effectiveness across tasks. We introduce ICONS, a gradient-based Influence CONsensus approach for vision-language data Selection. Our method leverages first-order training dynamics to estimate each example’s influence on validation performance, then aggregates these estimates across tasks via majority voting. This cross-task consensus identifies consistently valuable data points while mitigating score calibration and outlier sensitivity, enabling robust and scalable data selection for diverse multitask mixtures. Models trained on our selected 20% data subset from LLAVA-665K (respectively: from CAMBRIAN-7M, from VISION-FLAN-186K) retain 98.6% (respectively: 98.8%, 99.8%) of full-dataset performance. We demonstrate that our selected data generalizes to unseen tasks and model architectures, and release three compact subsets LLAVA-ICONS-133K, CAMBRIAN-ICONS-1.4M, and VISION-FLAN-ICONS-37K for efficient vision-language model development.

1. Introduction

Visual instruction tuning (VIT) is a crucial step in training vision-language models (VLMs) [1, 2], enabling them to follow language instructions grounded in visual content. Recent approaches rely on large-scale instruction following datasets such as LLAVA-665K [1] and CAMBRIAN-7M [3]. While effective, these datasets introduce significant barriers to model training and deployment: prolonged training times [4, 5], high storage demands [6, 7], and substantial compute costs [8, 9]. Moreover, not all training samples contribute equally to diverse downstream tasks and naively scaling up diverse data mixtures can introduce redundancy and inefficiency. This raises a fundamental question:

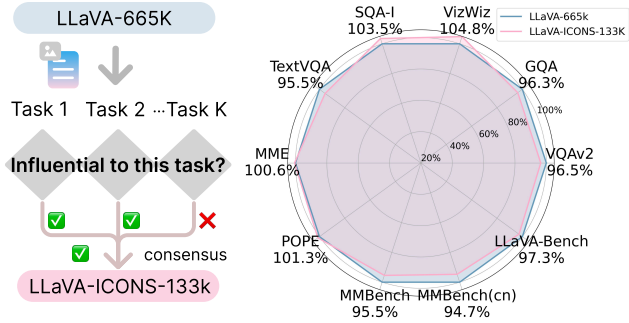


Figure 1. **Influence consensus for vision-language data selection.** (Left) Given a large-scale visual instruction tuning dataset (LLAVA-665K), our method uses majority voting across task-specific influence scores to identify training samples that are consistently influential across multiple tasks, forming a compact 20% subset (LLAVA-ICONS-133K) with data points achieving influence consensus. (Right) The radar plot compares performance between LLAVA-665K and our selected subset, showing the selected subset achieves comparable results to the full dataset.

Can we identify a compact, multitask-effective subset of training data that preserves model capabilities across tasks while enabling faster experimentation?

Prior work has explored various data selection strategies, including gradient-based approaches [10, 11], influence functions [12, 13], and diversity-based sampling [14, 15]. However, many of these methods either optimize for single tasks in isolation or maximize source diversity without aligning to downstream needs. In the context of VIT data that supports diverse vision-language tasks, this is particularly limiting: optimizing for one task may hurt generalization, and task-agnostic diversity may dilute impact. Rather than selecting data based on per-task influence, we aim to identify samples that are broadly useful, with training examples that consistently contribute across tasks. To do this, we aggregate gradient-based influence scores using a simple yet effective majority voting approach to reach influence consensus.

We introduce ICONS (Influence CONsensus vision-

language data Selection), a method that builds upon LESS [10], a gradient-based selection approach. Given access to validation data for each target task, our method: (1) computes first-order gradient influence scores to measure how each training sample impacts task-specific performance, and (2) reaches influence consensus via majority voting to identify training samples that show consistent positive impact across multiple tasks. This consensus-based mechanism identifies universally valuable training examples: while some samples might be highly influential for individual tasks, we prioritize those that demonstrate broad utility across the task spectrum. While the computational cost of influence estimation is high, this front-loaded, one-time investment yields a standardized, compact dataset that can significantly accelerate development of multimodal models, and enables reusable gradient datastores that amortize costs across iterations and deliver long-term savings.

Using ICONS, we create LLAVA-ICONS-133K, CAMBRIAN-ICONS-1.4M, and VISION-FLAN-ICONS-37K, automatically selected 20% subsets of LLAVA-665K [1], CAMBRIAN-7M [3], and VISION-FLAN-186K [16] datasets, respectively. These compact datasets maintain 98.6%, 98.8%, and 99.8% of their original performance across multiple vision-language tasks, providing significant improvements over randomly selecting same-sized subsets (95.8%, 95.4%, and 91.6%) and eliminating approximately two-thirds of the performance drop from shrinking the training data. Moreover, our ICONS outperforms all baselines across different selection ratios, and remarkably achieves above-full-dataset performance, surpassing the original datasets at a 60% selection ratio for LLAVA-665K. Importantly, the selected subsets show strong transferability, e.g., LLAVA-ICONS-133K maintains 95.5-113.9% relative performance across unseen tasks, suggesting that ICONS identifies fundamentally valuable training data. We summarize our key contributions:

1. We propose ICONS, a simple yet effective method for multitask vision-language data selection that identifies broadly valuable training examples via majority voting over task-specific gradient influence scores.
2. Our consensus-based selection outperforms all baselines (§4.2) and we ablate influence aggregation strategies and show the advantage of voting-based consensus (§4.3). ICONS exceeds 102% of full-dataset performance at a 60% selection ratio on LLAVA-665K (§4.5).
3. We release subsets LLAVA-ICONS-133K, CAMBRIAN-ICONS-1.4M and VISION-FLAN-ICONS-37K for resource-efficient development, demonstrating competitive performance including generalization to unseen tasks (§4.4) despite a 5x reduction in training data.

2. Related work

Visual instruction tuning. Vision-language models (VLMs), e.g., Flamingo [17], LLaVA [2], BLIP2 [18], and Cambrian [3], enable understanding and reasoning across visual and textual modalities for various multimodal tasks. A key component in advancing VLMs is visual instruction tuning (VIT) [2], a training process that enables these models to interpret and follow instructions within a vision-language context, transforming them into versatile multimodal assistants. This tuning process not only improves the models’ instruction-following abilities but also aligns their outputs more closely with user expectations, thus enhancing their utility in practical applications [2]. To support this paradigm, recent VIT datasets have scaled to contain hundreds of thousands to millions of instruction-response pairs [1, 3].

Data selection. Data selection methods [19] can be categorized based on the types of information they utilize for selection. Representation-based approaches [20, 21] leverage embeddings to capture data representations. Loss trajectory-based methods [22] prioritize data points that contribute most significantly to reducing generalization error over training. Gradient-based techniques [10, 11, 23] select data based on gradient information. Recent work has explored various approaches to select optimal visual instruction tuning datasets. Concurrent work TIVE [24] employs gradient-based selection to identify representative instances. TIVE assumes that the number of specialist data should be proportional to task difficulty and thus samples specialist data based on an estimation of task difficulty. Our method does not rely on this assumption – we directly select samples that benefit the greatest number of tasks. COINCIDE [21] clusters data based on representations associated with concept-skill compositions. Our work follows targeted instruction tuning selection approach LESS [10] to utilize gradient information to calculate the specialist influence (i.e., the influence on a specific task) and extends it to general scenarios by aggregating information across tasks and selecting data influential for multiple downstream tasks via majority voting.

3. ICONS: Influence CONsensus for vision-language data Selection

We propose a consensus-driven, gradient-based data selection framework (Fig. 2) for visual instruction tuning datasets. We formalize the problem setup in §3.1 and establish gradient-based influence estimation preliminaries in §3.2. Our two-stage data selection framework consists of: the *specialist* stage (§3.3), which computes task-specific influence scores, and the *generalist* stage (§3.4), which builds cross-task consensus through voting-based aggregation.

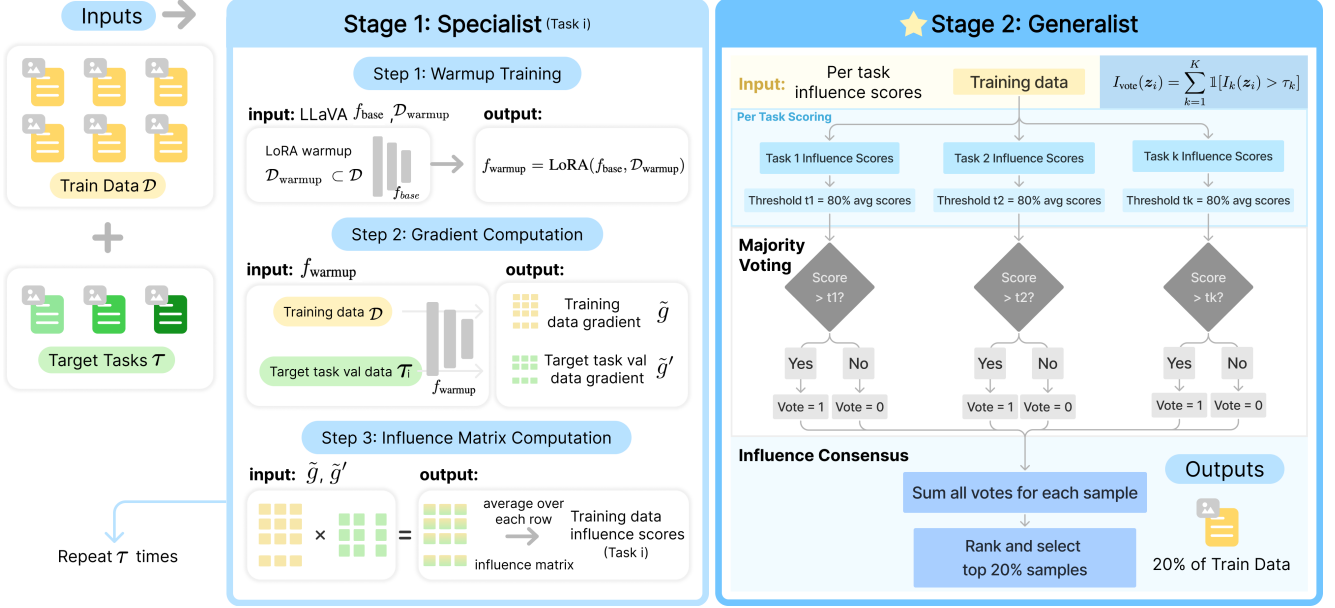


Figure 2. **ICONS**. The Specialist stage (*left*) processes each task through: (1) warmup training on a small subset, (2) gradient computation for training and validation data, and (3) influence matrix computation for per-task scores. The Generalist stage (*right*) performs **Influence Consensus** to aggregate information across tasks. For each task, samples scoring above a percentile threshold (e.g., 80th for 20% selection) receive a vote. Votes are summed across tasks, and samples with the highest vote counts are selected, creating a compact yet effective training dataset that performs well across all tasks.

3.1. Problem formulation

Given a large-scale visual instruction tuning dataset $\mathcal{D} = \{(\mathbf{I}_i, \mathbf{x}_i, \mathbf{y}_i)\}_{i=1}^N$ containing N samples, where each data point $\mathbf{z}_i = (\mathbf{I}_i, \mathbf{x}_i, \mathbf{y}_i)$ includes an image \mathbf{I}_i , natural language instruction \mathbf{x}_i , and corresponding target response \mathbf{y}_i ¹, and given access to validation data \mathcal{V}_k for each downstream task $T_k \in \mathcal{T} = \{T_1, \dots, T_K\}$, our goal is to select a compact subset $\mathcal{S} \subset \mathcal{D}$ of size $M \ll N$ that maximizes model performance across multiple downstream tasks.

Concretely, we let $f_{\mathcal{S}}$ and $f_{\mathcal{D}}$ denote models trained on subset \mathcal{S} and full dataset \mathcal{D} , respectively, and $\text{Score}(f, T_k)$ be the task-specific evaluation score achieved by model f on task T_k . $\text{Rel}(f_{\mathcal{S}}, T_k) = \frac{\text{Score}(f_{\mathcal{S}}, T_k)}{\text{Score}(f_{\mathcal{D}}, T_k)}$ quantifies the subset-trained model’s performance relative to that of the model trained on the entire dataset, with values close to 1 indicating that the subset maintains the performance of full training [21]. Our goal is then to identify the subset:

$$\mathcal{S}^* = \arg \max_{\mathcal{S} \subset \mathcal{D}, |\mathcal{S}|=M} \sum_{k=1}^K \text{Rel}(f_{\mathcal{S}}, T_k). \quad (1)$$

We define the average relative performance across all tasks as $\mathbf{Rel.} = \sum_{k=1}^K \text{Rel}(f_{\mathcal{S}}, T_k)/K$, and our objective is to select a subset where $\mathbf{Rel.} \approx 1$, i.e., the model trained on the subset achieves comparable performance to the one trained with full dataset.

¹This framework supports multi-turn conversational data, yet we formalize the setup for single-turn instruction-tuning for clarity and simplicity.

3.2. Preliminaries

Building on the problem formulation in §3.1, we formalize how to estimate the influence of training samples on downstream task performance. Since our goal is to maximize $\text{Rel}(f_{\mathcal{S}}, T_k)$ across tasks as defined in Eqn. 1, we need an efficient way to estimate how each training sample contributes to the $\text{Score}(f_{\mathcal{S}}, T_k)$ term in the numerator. Denote a training data point as \mathbf{z} and a validation data point as \mathbf{z}' from validation set \mathcal{V}_k for task T_k . Following [10, 25], we estimate how $\mathbf{z} \in \mathcal{D}$ affects validation loss by measuring its gradient alignment with reducing validation loss on \mathcal{V}_k , which directly impacts task-specific evaluation. When training with SGD and batch size 1, using data point \mathbf{z} at timestep t leads to a model update $\theta_{t+1} = \theta_t - \eta_t \nabla \ell(\mathbf{z}; \theta_t)$, where η_t is the learning rate. To reduce the computational cost, we use the first-order Taylor expansion to estimate the loss on a given validation data point \mathbf{z}' at time step $t+1$ as:

$$\ell(\mathbf{z}'; \theta_{t+1}) \approx \ell(\mathbf{z}'; \theta_t) + \langle \nabla \ell(\mathbf{z}'; \theta_t), \theta_{t+1} - \theta_t \rangle.$$

Training sample \mathbf{z} ’s influence on validation sample \mathbf{z}' is:

$$\begin{aligned} \mathcal{I}_t(\mathbf{z} \rightarrow \mathbf{z}') &= \ell(\mathbf{z}'; \theta_{t+1}) - \ell(\mathbf{z}'; \theta_t) \\ &\approx -\eta_t \langle \nabla \ell(\mathbf{z}'; \theta_t), \nabla \ell(\mathbf{z}; \theta_t) \rangle, \end{aligned}$$

which we refer to as an influence score. The gradient-based selection approach selects training samples $\{\mathbf{z}\}$ that max-

imize the gradient inner product $\langle \nabla \ell(\mathbf{z}'; \boldsymbol{\theta}_t), \nabla \ell(\mathbf{z}; \boldsymbol{\theta}_t) \rangle^2$ through a greedy, first-order approximation, which leads to larger reductions in validation loss for point \mathbf{z}' . While it omits second-order terms compared to influence functions [13], it provides an efficient approximation to rank the impact of training samples [10].

3.3. Specialist: individual task influence ranking

To rank the influence of training data for each target task, we compute the influence score of each training data point on a validation set that represents the target task distribution. Following LESS [10], the process involves three steps: (1) training the model on 5% randomly selected data as a lightweight warm-up to initialize visual instruction-following capabilities, (2) computing gradients for training and validation data and compressing the gradients via random projection, and (3) computing the influence score to quantify the impact of each training data on validation set.

Step 1: Warm-up Training. Following LESS [10], we apply LoRA [26] on a small random subset $\mathcal{D}_{\text{warmup}} \subset \mathcal{D}$ (5%) to obtain $f_{\text{warmup}} = \text{LoRA}(f_{\text{base}}, \mathcal{D}_{\text{warmup}})$, which develops basic visual instruction-following capabilities.

Step 2: Gradient computation. For each training data $\mathbf{z}_i \in \mathcal{D}$ and validation data $\mathbf{z}'_j \in \mathcal{D}_{\text{val}}^k$ from \mathcal{T}_k , we compute their gradients with respect to f_{warmup} parameters $\boldsymbol{\theta}_w$:

$$g_i = \nabla_{\boldsymbol{\theta}_w} \mathcal{L}(f_{\text{warmup}}(\mathbf{z}_i), \mathbf{y}_i), \quad g'_j = \nabla_{\boldsymbol{\theta}_w} \mathcal{L}(f_{\text{warmup}}(\mathbf{z}'_j), \mathbf{y}'_j)$$

where \mathbf{y}_i and \mathbf{y}'_j are the targets for \mathbf{z}_i and \mathbf{z}'_j , respectively. In order to reduce computational and storage overhead, we apply random projection to the gradient feature: $\tilde{g}_i = Rg_i$ and $\tilde{g}'_j = Rg'_j$, where $R \in \mathbb{R}^{d' \times d}$ is a random projection matrix with $d' \ll d$ that preserves inner products with high probability [27]. We further normalize the projected gradients, $\tilde{g}_i = \frac{\tilde{g}_i}{\|\tilde{g}_i\|_2}$, $\tilde{g}'_j = \frac{\tilde{g}'_j}{\|\tilde{g}'_j\|_2}$ to prevent bias from sequence length differences [10].

Step 3: Influence matrix computation. We compute the influence matrix $I \in \mathbb{R}^{|\mathcal{D}| \times |\mathcal{D}_{\text{val}}^k|}$ where each entry $I_{ij} = \langle \tilde{g}_i, \tilde{g}'_j \rangle$ is the influence of the training data \mathbf{z}_i on the validation data \mathbf{z}'_j , following the setting in LESS [10], we take the average influence of training data \mathbf{z}_i across all validation examples on the target task k to obtain a representative task-level influence score:

$$\bar{I}_k(\mathbf{z}_i) = \frac{1}{|\mathcal{D}_{\text{val}}^k|} \sum_{j=1}^{|\mathcal{D}_{\text{val}}^k|} I_{ij}. \quad (2)$$

This influence estimation process provides a task-specific ranking for the training set \mathcal{D} with respect to task \mathcal{T}_k , where

²In practice, we use cosine similarity instead of direct inner products to avoid biasing selection toward shorter sequences, since gradient norms tend to be inversely correlated with sequence length as noted in [10].

a higher influence score \bar{I}_i suggests a higher influence on \mathcal{T}_k . We can select a small training subset \mathcal{S}_k for a given task k by selecting the training examples \mathbf{z}_i with the highest-influence values $\bar{I}_k(\mathbf{z}_i)$. This simple greedy approach has been shown by LESS to be successful, and thus we use it as our task-specific (“specialist”) baseline. However, recall that our goal is to select a single compact subset that maximizes the performance across *all* tasks. We address this disconnection between task-specific rankings and overall optimization by proposing a voting-based generalist approach to identify the most broadly impactful training data.

3.4. Generalist: cross-task influence consensus

Our goal is to identify a training set subset $\mathcal{S} \subset \mathcal{D}$ of size $M \ll N$ such that its performance across all tasks remains high as defined by Eqn. 1. There are multiple ways to tackle this, depending on the assumptions one makes about the task-specific influence scores $\bar{I}_k(\mathbf{z}_i)$. The simplest approach is to merge together all the different tasks’ validation sets $\mathcal{D}_{\text{val}}^k$ (normalizing for their different sizes) and compute the total influence score for a training example \mathbf{z}_i as:

$$I_{\text{Merge}}(\mathbf{z}_i) = \sum_{k=1}^K \bar{I}_k(\mathbf{z}_i). \quad (3)$$

LESS [10] suggests a similar approach:

$$I_{\text{Max}}(\mathbf{z}_i) = \max_{k=1, \dots, K} \bar{I}_k(\mathbf{z}_i), \quad (4)$$

i.e., the influence of the data is measured as its *highest* influence on any tasks. The set of M training examples with the highest aggregated influence scores would be selected for inclusion in the training set $\mathcal{S}_{\text{merge}}$ (correspondingly, \mathcal{S}_{max}). Both approaches, however, require that the influence scores \bar{I}_k be well-calibrated across the different tasks; as we show in §4.3 this may not necessarily be the case.

An alternative approach which does not require directly comparing influence scores \bar{I}_k across tasks k is to leverage the relative rank of the training examples within each task. Concretely, we compute $\text{rank}_k(\mathbf{z}_i)$ for each example \mathbf{z}_i relative to other examples for task k according to their influence scores (higher influence scores correspond to lower rank). We can have a couple of options. First, we can select the training subset either using the Round Robin (RR) approach [28] where we iterate over tasks and select the lowest-rank example which has not yet been selected to add to our set \mathcal{S}_{RR} . Alternatively, we can select the training subset $\mathcal{S}_{\text{MinRank}}$ such that all the examples within it have a low rank for some task k . Mathematically, albeit somewhat confusingly, this corresponds to:

$$\mathcal{S}_{\text{MinRank}} = \arg \max_{\mathcal{S} \subset \mathcal{D}, |\mathcal{S}|=M} \min_{\substack{\text{task } k \\ \text{example } \mathbf{z}_i \notin \mathcal{S}}} \text{rank}_k(\mathbf{z}_i), \quad (5)$$

i.e., all examples that are *not* included in \mathcal{S} would have high relative ranks $\text{rank}_k(\mathbf{z}_i)$ for all tasks k . However, this approach ignores the potential interplay between tasks. Since Eqn. 1 maximizes the *sum* of relative performance across tasks k , if a training example is beneficial for multiple tasks, we may want to include it even at the expense of lower-ranked examples for individual tasks. Thus, we introduce a consensus-based voting strategy that identifies training samples consistently showing high influence across tasks. For each task k , we set a threshold τ_k at the $((1-p) \times 100)$ -th percentile of the influence score distribution, where p represents the selection ratio ($p = 0.2$ in our main experiments). A sample \mathbf{z}_i is considered important for task k if $\bar{I}_k(\mathbf{z}_i) \geq \tau_k$. We define the voting-based influence score as:

$$I_{\text{vote}}(\mathbf{z}_i) = \sum_{k=1}^K \mathbb{1}[\bar{I}_k(\mathbf{z}_i) \geq \tau_k], \quad (6)$$

where $\mathbb{1}[\cdot]$ is the indicator function. The final score ranges from 0 (no importance for any task) to K (consistent importance for all tasks). Equivalently, we can define the threshold-based specialist sets as: $\mathcal{S}_k = \{\mathbf{z}_i \in \mathcal{D} : \bar{I}_k(\mathbf{z}_i) \geq \tau_k\}$. We then select the combined training set as:

$$\mathcal{S}_{\text{ICONS}} = \arg \max_{\mathcal{S} \subset \mathcal{D}, |\mathcal{S}|=M} \sum_{k=1}^K \sum_{\mathbf{z}_i \in \mathcal{S}} \mathbb{1}[\mathbf{z}_i \in \mathcal{S}_k] \quad (7)$$

$$= \arg \max_{\mathcal{S} \subset \mathcal{D}, |\mathcal{S}|=M} \sum_{\mathbf{z}_i \in \mathcal{S}} I_{\text{vote}}(\mathbf{z}_i) \quad (8)$$

This simple approach offers a key advantage: it does not rely on calibration of influence scores across tasks, and does not make any a-priori assumptions about the relationship between tasks (e.g., that every task needs to have its highest-scoring examples included in the combined training set). Our generalist stage converts each task’s ranked list into a binary vote (“above threshold” or not) and then combines these votes across tasks, eliminating the need for task-specific normalization. As a result, the selection remains insensitive to scale differences while still capturing relative importance within each task. Meanwhile, a training sample is selected only when several tasks independently rank it as influential, preventing over-representation of single-task outliers and ensuring the cross-task utility.

4. Experiments

We first discuss our experiment setup (§4.1), then compare ICONS with state-of-the-art methods (§4.2) and analyze different selection strategies (§4.3). We evaluate transferability to unseen tasks (§4.4), performance across selection ratios (§4.5), vote distributions (§4.6), and characteristics of low-vote samples (§4.7).

4.1. Evaluation test-bed

Datasets & model. We apply ICONS on major VIT training datasets: LLaVA-665K [1], CAMBRIAN-7M [3] and VISION-FLAN-186K [16]. The majority of our analysis and ablation experiments are conducted on LLaVA-665K. For our experiments, we use the LLaVA-v1.5 model [1] checkpoint after Stage 1 (pre-training for feature alignment) as defined in the original LLaVA training pipeline, with a default size of 7B parameters and LLaVA-665K unless otherwise specified. This checkpoint³ corresponds to the model after training the projector but before any visual instruction tuning in Stage 2. Importantly, this model has not been exposed to the LLaVA-665K VIT dataset prior to the data selection process. In all experiments, we train the models for one epoch following the official finetuning hyperparameters using LoRA. More details on computation, including hardware specifications and runtime, are in Appendix §A.

Target tasks. We evaluate ICONS across diverse multimodal benchmarks (details are in Appendix §B, Tab. 6) that test different capabilities of vision-language models: 1) Multiple-choice understanding: MMBench [29] and MME [30]⁴ 2) Visual question answering: VQAv2 [31], GQA [32], and VizWiz [33]; 3) Text understanding in images: TextVQA [34]; 4) Scientific reasoning: ScienceQA [35]; 5) Open-ended generation: LLaVA-W Bench [2]; 6) Factual consistency: POPE [36].

Baselines. We compare our ICONS against several baselines, including random selection, CLIP-Score [37] for measuring image-text alignment, EL2N [23] based on embedding L2 norms, and Perplexity [38] using language model scores. We also compare against SemDeDup [20] for semantic deduplication and D2-Pruning [39] for distribution-aware pruning. Additional baselines include Self-Sup [40] leveraging self-supervised signals, while Self-Filter [41] and COINCIDE [21] are designed for vision-language data selection. We reference LLaVA-665K baseline results from COINCIDE [21]. Additionally, we compare with representation-based data selection approach (RDS) [10, 28].

4.2. Main results

LLAva-665K selection. As shown in Tab. 1, ICONS achieves the best overall performance with 98.6% Rel. on LLaVA-665K, outperforming all baselines with LLaVA-ICONS-133K, 20% of the training data. Remarkably, we achieve comparable or better performance than full dataset training on several tasks: SQA-I (70.8 vs. 68.4), MME (1485.7 vs. 1476.9) and POPE (87.5 vs. 86.4). While COINCIDE achieves strong performance (97.4% Rel.), it

³llava-v1.5-mlp2x-336px-pretrain-vicuna-7b-v1.5, which has no prior exposure to the visual instruction tuning data.

⁴For MME, we focus on its perception section following [21], which evaluates vision capabilities.

Table 1. **Selection results on LLAVA-665K.** Performance comparison of different data selection approaches when trained on 20% of the LLAVA-665K dataset. Tasks are ordered by random selection’s relative performance. The best and second best results for each benchmark are shown in **bold** and underlined, respectively. Our method ICONS achieves the highest overall Rel. (98.6%), consistently outperforming existing approaches including COINCIDE [21] (97.4%) and D2-Pruning [39] (94.8%).

Method	MME	SQA-I	POPE	VQAv2	LLaVA-W Bench	TextVQA	MMBench en	GQA	VizWiz	Rel. (%)
Full	1476.9	68.4	86.4	79.1	67.9	58.2	66.1	58.9	63.0	47.8
Random	1483.0	68.5	84.7	75.7	65.0	55.3	62.2	54.8	58.9	44.3
CLIP-Score [37]	1331.6	65.0	85.3	73.4	66.2	54.7	55.2	52.0	51.4	43.0
EL2N [23]	1439.5	65.5	84.3	76.2	64.9	53.0	53.2	47.4	58.7	43.7
Perplexity [38]	1341.4	65.1	82.6	75.8	<u>68.3</u>	52.8	52.0	45.8	57.0	47.8
SemDeDup [20]	1376.9	65.8	84.7	74.2	70.0	<u>55.5</u>	52.2	48.5	54.5	46.9
D2-Pruning [39]	1391.2	<u>69.3</u>	85.7	73.0	63.9	51.8	65.7	57.6	58.4	41.9
Self-Sup [40]	1335.9	67.8	83.5	74.9	63.3	49.3	61.4	53.8	59.5	46.0
Self-Filter [41]	1306.2	61.4	83.8	73.7	64.9	52.9	48.8	45.3	58.3	53.2
COINCIDE [21]	1495.6	69.2	86.1	76.5	67.3	55.6	<u>63.1</u>	54.5	<u>59.8</u>	46.8
RDS [10, 28]	1393.8	68.0	<u>86.3</u>	75.1	63.7	54.9	61.2	52.7	57.9	48.6
ICONS (ours)	<u>1485.7</u>	70.8	87.5	<u>76.3</u>	66.1	55.6	<u>63.1</u>	<u>55.8</u>	60.7	<u>50.1</u>
										98.6

falls short of ICONS on key tasks. Approaches like EL2N, Perplexity, SemDeDup achieve only 91-92% Rel., showing limitations in preserving performance.

CAMBRIAN-7M & VISION-FLAN-186K selection. We provide results on VISION-FLAN-186K [16] and CAMBRIAN-7M [3] in Tab. 2. On VISION-FLAN-186K, our method achieves near-full performance (99.8% Rel.) using just 37k samples, significantly outperforming random selection (91.6%). Similarly, on CAMBRIAN-7M, ICONS maintains strong performance (98.8% Rel.) with 1,414k samples, while random selection achieves 95.4%. These results demonstrate our approach works effectively on both small and large datasets, consistently preserving model capabilities while drastically reducing training data.

Comparisons with representation-based data selection. We compare against **RDS** (Representation-based Data Selection) [10, 28], a strong baseline in language-only data selection. RDS computes training-validation similarity using final-layer representation of the last token in each sequence instead of gradients. For a fair comparison, we use the same influence matrix formulation (Eqn. 2) and apply majority voting. Our method consistently outperforms RDS across all tasks, particularly those requiring perceptual grounding – e.g., higher scores on GQA (60.7 vs. 57.9), SQA-I (70.8 vs. 68.0), and MME (1485.7 vs. 1393.8). While RDS is effective for text-only data (e.g. TULU-2/3 [42, 43]), vision-language tasks demand alignment between modalities, where representation similarity is limited as it only reflects current embedding proximity, whereas gradient-based approaches directly estimate each sample’s contribution to validation loss, better capturing cross-modal training dynamics. We further provide qualitative comparisons in Appendix §F.

4.3. Analysis of aggregation strategies

Ablations. As introduced in §3.4, we explore multiple strategies for aggregating task-specific influence rankings into a single compact subset. We compare our majority voting approach (**Vote**) with score-based methods (**Merge**, **Max**, and normalized variants (**Merge-SumNorm**, **Merge-GausNorm**)) and rank-based methods (**Round Robin**, **Min-Rank**). Our approach outperforms all alternatives (Tab. 3; full results in Appendix Tab. 5), achieving 98.6% Rel. Our majority voting effectively identifies consistently influential examples without requiring score calibration across tasks.

Limitations of score-based aggregation. Score-based methods like **Merge** (Eqn. 3) and **Max** (Eqn. 4) assume calibrated influence scores across tasks, which is rarely the case. We observe substantial variation in influence score distributions across tasks with standard deviations spanning from 8.15×10^{-3} (MME) to 1.26×10^{-3} (VQAv2), indicating that influence scores for MME are much more spread out, while those for VQAv2 are tightly concentrated. Similarly, mean influence scores vary in both magnitude and sign: MME has a relatively high positive mean (1.68×10^{-3}), while tasks like POPE (-2.83×10^{-4}) and GQA (-8.89×10^{-5}) have negative means. These patterns show certain tasks have wider influence scores distributions, making a sample helpful for one task but neutral or harmful for another. Aggregating raw scores biases selection toward tasks with higher variance or skewed means. To address this calibration issue, we experiment with normalization: **Merge-SumNorm**, which rescales each task’s influence scores by dividing them by a task-specific normalization factor (i.e., sum), and **Merge-GausNorm**, which normalizes the scores using task-wise mean and standard deviation before averaging:

Table 2. **Selection results on VISION-FLAN-186K and CAMBRIAN-7M.** Performance comparison of different data selection approaches when trained on 20% of the VISION-FLAN-186K [16] and CAMBRIAN-7M [3] datasets. ICONS achieves strong performance (99.8% and 98.8% Rel. respectively) while using only 20% of the training data, significantly outperforming random selection which is one of the strongest baselines, and approaching full performance.

Dataset	#Data	Method	VQAv2	GQA	VizWiz	SQA-I	TextVQA	POPE	MME	MMBench	LLaVA-W	Rel. (%)	
VISION-FLAN-186K	186k	Full	68.0	49.2	41.7	60.8	50.4	83.4	1,263.2	52.6	45.9	63.3	100.0
	27k	Random	64.1	45.8	37.5	58.7	45.3	82.9	1,079.8	46.5	39.6	58.7	91.6
	27k	ICONS (ours)	67.4	48.8	44.1	60.2	49.9	83.0	1,252.5	51.9	45.4	63.1	99.8
CAMBRIAN-7M	7,068k	Full	80.2	62.9	58.4	75.3	60.9	86.5	1,524.6	69.1	58.9	67.6	100.0
	1,414k	Random	74.2	57.5	61.9	71.0	57.1	86.4	1,465.7	63.3	49.6	70.4	95.4
		ICONS (ours)	79.6	62.1	60.7	73.9	59.8	86.2	1,503.1	67.8	55.8	67.0	98.8

Table 3. **Comparison of aggregation approaches.** Relative performance of different influence aggregation methods when selecting 20% of the LLaVA-665K dataset on the ten tasks from Tables 1 and 2. Our **Vote** achieves the best performance (98.6% Rel.), outperforming score-based, their normalized variants, and rank-based baselines. See Appendix Tab. 5 for per-task results.

Type	Score-based		Normalized Score-based	
	Merge	Max	Merge-GausNorm	Merge-SumNorm
Method	96.4	96.1	96.8	95.3
Type	Rank-based		Vote-based	
Method	Round Robin	MinRank	ICONS (ours)	
Rel. (%)	96.7	97.1	98.6	

$$I_{\text{Merge-SumNorm}}(\mathbf{z}_i) = \sum_{k=1}^K \frac{I_k(\mathbf{z}_i)}{\sum_j I_k(\mathbf{z}_j)}$$

$$I_{\text{Merge-GausNorm}}(\mathbf{z}_i) = \sum_{k=1}^K \frac{I_k(\mathbf{z}_i) - \mu_k}{\sigma_k}$$

However, as shown in Tab. 3, both methods still underperform compared to our voting-based strategy, reinforcing the limitations of relying on score magnitudes directly.

Limitations of rank-based aggregation. Rank-based methods sidestep the challenge of comparing raw influence scores by focusing on within-task ranking. **Round Robin** selects samples by cycling through each task and picking the highest-scoring remaining sample for that task, ensuring balanced coverage. **MinRank** (Eqn. 5) selects samples that have the best minimum rank across all tasks, prioritizing examples that perform exceptionally well in at least one task regardless of their performance in others. Although these methods ensure balanced coverage across tasks, they can overfit to outlier tasks. This is particularly evident with LLaVA-W Bench [2], which is an outlier in its influence ranking: both Round Robin and MinRank achieve relatively high scores on it (e.g. MinRank: 68.4) but at the cost of lower performance on all other tasks (Tab. 3). Rank-based selection can trade off overall efficacy on the mainstream tasks. In contrast, our **Vote** approach focuses on cross-task

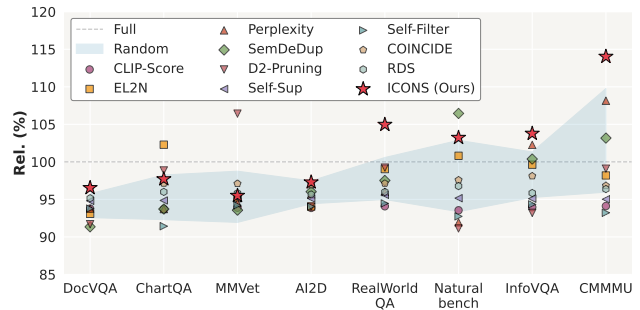


Figure 3. **Unseen task generalization across methods.** Performance on eight unseen benchmarks using 20% selected subsets, sorted by the average performance across 5 random selection runs (left: lower, right: higher). Shaded region shows mean and standard deviation across random runs. Our ICONS consistently outperforms all baselines. Full detailed results are in Appendix Tab. 7.

consensus rather than forcing equal representation, yielding better balance and higher overall performance (98.6% Rel.), showing the importance of identifying broadly influential examples rather than optimizing per-task rankings.

4.4. ICONS generalizes to unseen tasks

Data selected via ICONS demonstrate strong generalization on unseen benchmarks not used during data selection. In Fig. 3 and Appendix Tab. 7 we test LLaVA-ICONS-133K on diverse tasks including MMVet [44], NaturalBench [45], AI2D [46], ChartQA [47], DocVQA [48], InfoVQA [49], RealWorldQA [50] and CMMMU [51]. Notably, LLaVA-ICONS-133K achieves substantial improvements on challenging benchmarks (MMVet: 95.5%, AI2D: 97.3%) and even exceeds full dataset performance on harder tasks (CMMU: 114.0%, RealWorldQA: 104.4%, InfoVQA: 103.8%, NaturalBench: 103.2%), demonstrating superior generalization to entirely unseen task formats and domains despite these tasks not being included in the selection process. Importantly, LLaVA-ICONS-133K outperforms random selection across all benchmarks. This suggests that our selection approach successfully captures fundamental visual-language understanding capabilities that transfer well across different task formats and domains. We further provide the

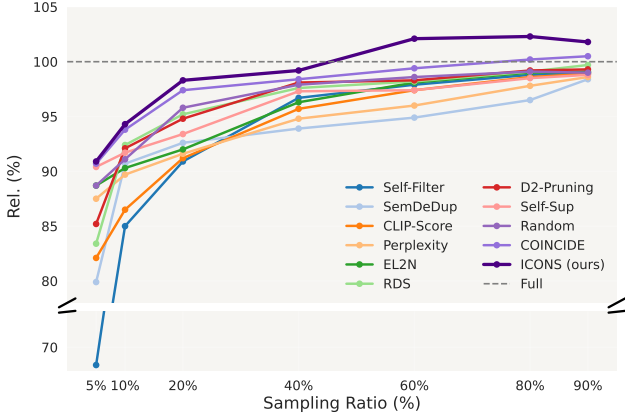


Figure 4. **Different selection ratios.** ICONS consistently outperforms all baselines across different selection ratios and remarkably exceeds 102% at a 60% selection ratio.

cross-architecture generalization results in Appendix §C.

4.5. ICONS outperforms baselines across ratios and exceeds full-data training at 60%

To understand how ICONS scales, we evaluate it across different selection ratios, progressively scaling the subset size from 5% to 90% of LLAVA-665K. As shown in Fig. 4, our results reveal several key patterns: First, ICONS shows particularly strong performance in the low-selection regime (5-20%), where identifying the most influential samples is crucial. Second, as the selection ratio increases, the performance gap between different methods gradually narrows. This convergence pattern is expected, as larger sample sizes naturally capture more of the dataset’s diversity and information. Despite this convergence trend, ICONS consistently outperforms all baselines across all selection ratios. Remarkably, it even surpasses full dataset performance at the 60% ratio, achieving over 102% relative score. One hypothesis is that ICONS can also effectively filter out potentially harmful or noisy training samples that might negatively impact model training, thereby surpassing the full training performance.

4.6. How does voting change with selection ratio?

We analyze vote distribution across selection ratios to understand task consensus patterns (Tab. 4, Appendix Fig. 6). At 5% selection, 72.1% of samples receive zero votes, indicating highly task-specific selection. As the ratio increases to 50% and 95%, the distribution shifts rightward with median votes rising to 4 and 5-7 respectively, and zero-vote samples decreasing to 8.3% and 1.2%. This rightward shift demonstrates that task consensus emerges as selection criteria relax, revealing samples with broader multi-task utility, while persistent zero-vote samples indicate universally low-quality or redundant data. These patterns validate our voting-based aggregation approach, which prioritizes samples with higher multi-task agreement. We further visualize zero-vote and one-vote samples in §4.7.

Table 4. **Vote distribution across selection ratios.** Vote distributions shift from task-specific selection at low ratios to broader consensus at high ratios.

Ratio	Mean (\pm Std)	Median	Max Votes	Zero-Vote	Threshold
5%	0.50 \pm 0.98	0	7	72.1%	3 votes
20%	2.00 \pm 1.56	2	7	28.4%	5 votes
50%	5.00 \pm 2.21	5	7	8.3%	6 votes
90%	9.00 \pm 1.84	9	10	1.2%	9 votes
95%	9.50 \pm 1.42	10	10	0.8%	10 votes

4.7. What do low-vote training samples look like?

To understand what samples are filtered out, we examine zero-vote and 1-vote samples at a 90% selection ratio for LLAVA-665K, where the majority of samples receive votes, making the remaining low-vote samples particularly indicative of low-quality data. Zero-vote samples do not rank in the top percentile for any task, while 1-vote samples are selected by only a single task-specific specialist. As shown in Appendix Fig. 10, these low-vote samples exhibit characteristics that explain their low selection frequency: (1) subjective questions lacking objective ground truth (e.g., “Is the woman pretty?”), (2) trivial questions providing minimal visual learning signal (e.g., “Is the door open?” with answer “Yes”), and (3) redundant questions about the same image content. By filtering out such potentially harmful or redundant examples, ICONS focuses training on more informative and generalizable samples, and thus exceeds full-dataset performance.

5. Conclusion

We introduce ICONS, an influence consensus-based approach for visual instruction tuning data selection. It leverages gradient-based influence estimation and aggregates task-level influence scores through majority voting to select training samples broadly beneficial across tasks. ICONS addresses limitations of prior approaches by avoiding assumptions about score comparability across tasks and reducing sensitivity to outlier task rankings that bias selection. ICONS builds compact, high-impact datasets achieving 98.6% of full performance using only 20% of LLAVA-665K while generalizing well to unseen tasks and architectures. Beyond data selection, it provides a principled way to reason about data influence in multitask mixtures. We release LLAVA-ICONS-133K, CAMBRIAN-ICONS-1.4M, and VISION-FLAN-ICONS-37K as compact 20% subsets maintaining strong performance, hoping to inspire further exploration into data-efficient vision-language models.

Limitations. Our approach’s main limitation is computational expense: computing gradients for large datasets is costly (Appendix §A), potentially constraining applicability to extremely large-scale data. To support the research community under resource constraints, we release the LLAVA-ICONS-133K dataset for iteration and model development.

Broader impact. While our work does not directly imply negative impacts, it may indirectly propagate biases present in the original datasets. Positively, it enables more efficient and sustainable model development by reducing data redundancy and computational cost while maintaining performance. Continued discussion on these aspects remains critical for data-efficient vision-language models.

Acknowledgments. This material is based upon work supported by the National Science Foundation under Grant No. 2107048 and No.2112562. Any opinions, findings, and conclusions, or recommendations expressed in this material are those of the author(s) and do not necessarily reflect the views of the National Science Foundation. This work is also supported by the Singapore National Research Foundation and the National AI Group in the Singapore Ministry of Digital Development and Information under the AI Visiting Professorship Programme (award number AIVP-2024-001). We thank many people for their helpful discussion and feedback, listed in alphabetical order by last name: Allison Chen, Hee Seung Hwang, Hamish Ivison, Carlos E. Jimenez, Polina Kirichenko, Jae-woo Lee, Zhiqiu Lin, Tiffany Ling, Shengbang Tong, Ethan Tseng, Esin Tureci, Justin Wang, Zirui Wang.

References

- [1] Haotian Liu, Chunyuan Li, Yuheng Li, and Yong Jae Lee. Improved baselines with visual instruction tuning. In *Proceedings of the IEEE/CVF Conference on Computer Vision and Pattern Recognition*, pages 26296–26306, 2024. [1](#), [2](#), [5](#)
- [2] Haotian Liu, Chunyuan Li, Qingyang Wu, and Yong Jae Lee. Visual instruction tuning. *Advances in neural information processing systems*, 36, 2024. [1](#), [2](#), [5](#), [7](#), [14](#), [29](#)
- [3] Shengbang Tong, Ellis Brown, Penghao Wu, Sanghyun Woo, Manoj Middepogu, Sai Charitha Akula, Jihan Yang, Shusheng Yang, Adithya Iyer, Xichen Pan, et al. Cambrian-1: A fully open, vision-centric exploration of multimodal llms. *arXiv preprint arXiv:2406.16860*, 2024. [1](#), [2](#), [5](#), [6](#), [7](#), [14](#), [15](#)
- [4] Tom Brown, Benjamin Mann, Nick Ryder, Melanie Subbiah, Jared D Kaplan, Prafulla Dhariwal, Arvind Neelakantan, Pranav Shyam, Girish Sastry, Amanda Askell, et al. Language models are few-shot learners. *Advances in neural information processing systems*, 33:1877–1901, 2020. [1](#)
- [5] Jared Kaplan, Sam McCandlish, Tom Henighan, Tom B Brown, Benjamin Chess, Rewon Child, Scott Gray, Alec Radford, Jeffrey Wu, and Dario Amodei. Scaling laws for neural language models. *arXiv preprint arXiv:2001.08361*, 2020. [1](#)
- [6] Samyam Rajbhandari, Jeff Rasley, Olatunji Ruwase, and Yuxiong He. Zero: Memory optimizations toward training trillion parameter models. In *SC20: International Conference for High Performance Computing, Networking, Storage and Analysis*, pages 1–16. IEEE, 2020. [1](#)
- [7] Samir Yitzhak Gadre, Gabriel Ilharco, Alex Fang, Jonathan Hayase, Georgios Smyrnis, Thao Nguyen, Ryan Marten, Mitchell Wortsman, Dhruba Ghosh, Jieyu Zhang, et al. Data-comp: In search of the next generation of multimodal datasets. *Advances in Neural Information Processing Systems*, 36, 2024. [1](#)
- [8] Pratyush Maini, Skyler Seto, He Bai, David Grangier, Yizhe Zhang, and Navdeep Jaitly. Rephrasing the web: A recipe for compute and data-efficient language modeling. *arXiv preprint arXiv:2401.16380*, 2024. [1](#)
- [9] Carole-Jean Wu, Ramya Raghavendra, Udit Gupta, Bilge Acun, Newsha Ardalani, Kiwan Maeng, Gloria Chang, Fiona Aga, Jinshi Huang, Charles Bai, et al. Sustainable ai: Environmental implications, challenges and opportunities. *Proceedings of Machine Learning and Systems*, 4:795–813, 2022. [1](#)
- [10] Mengzhou Xia, Sadhika Malladi, Suchin Gururangan, Sanjeev Arora, and Danqi Chen. Less: Selecting influential data for targeted instruction tuning. *arXiv preprint arXiv:2402.04333*, 2024. [1](#), [2](#), [3](#), [4](#), [5](#), [6](#)
- [11] Zhiwei Deng, Tao Li, and Yang Li. Influential language data selection via gradient trajectory pursuit. *arXiv preprint arXiv:2410.16710*, 2024. [1](#), [2](#)
- [12] Shuo Yang, Zeke Xie, Hanyu Peng, Min Xu, Mingming Sun, and Ping Li. Dataset pruning: Reducing training data by examining generalization influence. *arXiv preprint arXiv:2205.09329*, 2022. [1](#)
- [13] Pang Wei Koh and Percy Liang. Understanding black-box predictions via influence functions. In *International confer-*

ence on machine learning, pages 1885–1894. PMLR, 2017. 1, 4

[14] Simon Yu, Liangyu Chen, Sara Ahmadian, and Marzieh Fadaee. Diversify and conquer: Diversity-centric data selection with iterative refinement. *arXiv preprint arXiv:2409.11378*, 2024. 1

[15] Alexander Bukharin and Tuo Zhao. Data diversity matters for robust instruction tuning. *arXiv preprint arXiv:2311.14736*, 2023. 1

[16] Zhiyang Xu, Chao Feng, Rulin Shao, Trevor Ashby, Ying Shen, Di Jin, Yu Cheng, Qifan Wang, and Lifu Huang. Vision-flan: Scaling human-labeled tasks in visual instruction tuning. *arXiv preprint arXiv:2402.11690*, 2024. 2, 5, 6, 7

[17] Jean-Baptiste Alayrac, Jeff Donahue, Pauline Luc, Antoine Miech, Iain Barr, Yana Hasson, Karel Lenc, Arthur Mensch, Katherine Millican, Malcolm Reynolds, et al. Flamingo: a visual language model for few-shot learning. *Advances in Neural Information Processing Systems*, 35:23716–23736, 2022. 2

[18] Junnan Li, Dongxu Li, Silvio Savarese, and Steven Hoi. Blip-2: Bootstrapping language-image pre-training with frozen image encoders and large language models. *arXiv preprint arXiv:2301.12597*, 2023. 2

[19] Zayd Hammoudeh and Daniel Lowd. Training data influence analysis and estimation: A survey. *Machine Learning*, 113(5):2351–2403, 2024. 2

[20] Amro Abbas, Kushal Tirumala, Dániel Simig, Surya Ganguli, and Ari S Morcos. Semdedup: Data-efficient learning at web-scale through semantic deduplication. *arXiv preprint arXiv:2303.09540*, 2023. 2, 5, 6

[21] Jaewoo Lee, Boyang Li, and Sung Ju Hwang. Concept-skill transferability-based data selection for large vision-language models. *arXiv preprint arXiv:2406.10995*, 2024. 2, 3, 5, 6

[22] Sören Mindermann, Jan M Brauner, Muhammed T Razzak, Mrinank Sharma, Andreas Kirsch, Winnie Xu, Benedikt Höltgen, Aidan N Gomez, Adrien Morisot, Sebastian Farquhar, et al. Prioritized training on points that are learnable, worth learning, and not yet learnt. In *International Conference on Machine Learning*, pages 15630–15649. PMLR, 2022. 2

[23] Mansheej Paul, Surya Ganguli, and Gintare Karolina Dzigaite. Deep learning on a data diet: Finding important examples early in training. *Advances in neural information processing systems*, 34:20596–20607, 2021. 2, 5, 6

[24] Zikang Liu, Kun Zhou, Wayne Xin Zhao, Dawei Gao, Yaliang Li, and Ji-Rong Wen. Less is more: Data value estimation for visual instruction tuning. *arXiv preprint arXiv:2403.09559*, 2024. 2

[25] Garima Pruthi, Frederick Liu, Satyen Kale, and Mukund Sundararajan. Estimating training data influence by tracing gradient descent. *Advances in Neural Information Processing Systems*, 33:19920–19930, 2020. 3

[26] Edward J Hu, Yelong Shen, Phillip Wallis, Zeyuan Allen-Zhu, Yuanzhi Li, Shean Wang, Lu Wang, and Weizhu Chen. Lora: Low-rank adaptation of large language models. *arXiv preprint arXiv:2106.09685*, 2021. 4

[27] William B Johnson. Extensions of lipshitz mapping into hilbert space. In *Conference modern analysis and probability*, 1984, pages 189–206, 1984. 4

[28] Hamish Ivison, Muru Zhang, Faeze Brahman, Pang Wei Koh, and Pradeep Dasigi. Large-scale data selection for instruction tuning. *arXiv preprint arXiv:2503.01807*, 2025. 4, 5, 6

[29] Yuanhan Zhang Bo Li-Songyang Zhang, Wangbo Zhao Yike Yuan Jiaqi Wang, Conghui He Ziwei Liu Kai Chen, Dahua Lin Yuan Liu, and Haodong Duan. Mmbench: Is your multi-modal model an all-around player. *arXiv preprint arXiv:2307.06281*, 2, 2023. 5, 14, 27, 28

[30] Chaoyou Fu, Peixian Chen, Yunhang Shen, Yulei Qin, Mengdan Zhang, Xu Lin, Zhenyu Qiu, Wei Lin, Jinrui Yang, Xiawu Zheng, et al. Mme: a comprehensive evaluation benchmark for multimodal large language models. *corr abs/2306.13394* (2023), 2023. 5, 26

[31] Yash Goyal, Tejas Khot, Douglas Summers-Stay, Dhruv Batra, and Devi Parikh. Making the v in vqa matter: Elevating the role of image understanding in visual question answering. In *Proceedings of the IEEE conference on computer vision and pattern recognition*, pages 6904–6913, 2017. 5, 20

[32] Drew A Hudson and Christopher D Manning. Gqa: A new dataset for real-world visual reasoning and compositional question answering. In *Proceedings of the IEEE/CVF conference on computer vision and pattern recognition*, pages 6700–6709, 2019. 5, 21

[33] Danna Gurari, Qing Li, Abigale J Stangl, Anhong Guo, Chi Lin, Kristen Grauman, Jiebo Luo, and Jeffrey P Bigham. Vizwiz grand challenge: Answering visual questions from blind people. In *Proceedings of the IEEE conference on computer vision and pattern recognition*, pages 3608–3617, 2018. 5, 22

[34] Amanpreet Singh, Vivek Natarajan, Meet Shah, Yu Jiang, Xinlei Chen, Dhruv Batra, Devi Parikh, and Marcus Rohrbach. Towards vqa models that can read. In *Proceedings of the IEEE/CVF conference on computer vision and pattern recognition*, pages 8317–8326, 2019. 5, 24

[35] Pan Lu, Swaroop Mishra, Tanglin Xia, Liang Qiu, Kai-Wei Chang, Song-Chun Zhu, Oyvind Tafjord, Peter Clark, and Ashwin Kalyan. Learn to explain: Multimodal reasoning via thought chains for science question answering. *Advances in Neural Information Processing Systems*, 35:2507–2521, 2022. 5, 14, 23

[36] Yifan Li, Yifan Du, Kun Zhou, Jinpeng Wang, Wayne Xin Zhao, and Ji-Rong Wen. Evaluating object hallucination in large vision-language models. *arXiv preprint arXiv:2305.10355*, 2023. 5, 25

[37] Alec Radford, Jong Wook Kim, Chris Hallacy, Aditya Ramesh, Gabriel Goh, Sandhini Agarwal, Girish Sastry, Amanda Askell, Pamela Mishkin, Jack Clark, et al. Learning transferable visual models from natural language supervision. In *International conference on machine learning*, pages 8748–8763. PMLR, 2021. 5, 6

[38] Max Marion, Ahmet Üstün, Luiza Pozzobon, Alex Wang, Marzieh Fadaee, and Sara Hooker. When less is more: Investigating data pruning for pretraining llms at scale. *arXiv preprint arXiv:2309.04564*, 2023. 5, 6

[39] Adyasha Maharana, Prateek Yadav, and Mohit Bansal. D2 pruning: Message passing for balancing diversity and difficulty in data pruning. *arXiv preprint arXiv:2310.07931*, 2023. 5, 6

[40] Ben Sorscher, Robert Geirhos, Shashank Shekhar, Surya Gan-guli, and Ari Morcos. Beyond neural scaling laws: beating power law scaling via data pruning. *Advances in Neural Information Processing Systems*, 35:19523–19536, 2022. 5, 6

[41] Ruibo Chen, Yihan Wu, Lichang Chen, Guodong Liu, Qi He, Tianyi Xiong, Chenxi Liu, Junfeng Guo, and Heng Huang. Your vision-language model itself is a strong filter: Towards high-quality instruction tuning with data selection. *arXiv preprint arXiv:2402.12501*, 2024. 5, 6

[42] Hamish Ivison, Yizhong Wang, Valentina Pyatkin, Nathan Lambert, Matthew Peters, Pradeep Dasigi, Joel Jang, David Wadden, Noah A Smith, Iz Beltagy, et al. Camels in a changing climate: Enhancing lm adaptation with tulu 2. *arXiv preprint arXiv:2311.10702*, 2023. 6

[43] Nathan Lambert, Jacob Morrison, Valentina Pyatkin, Shengyi Huang, Hamish Ivison, Faeze Brahman, Lester James V Miranda, Alisa Liu, Nouha Dziri, Shane Lyu, et al. T\ ulu 3: Pushing frontiers in open language model post-training. *arXiv preprint arXiv:2411.15124*, 2024. 6

[44] Weihao Yu, Zhengyuan Yang, Linjie Li, Jianfeng Wang, Kevin Lin, Zicheng Liu, Xinchao Wang, and Lijuan Wang. Mm-vet: Evaluating large multimodal models for integrated capabilities. *arXiv preprint arXiv:2308.02490*, 2023. 7

[45] Baiqi Li, Zhiqiu Lin, Wenxuan Peng, Jean de Dieu Nyandwi, Daniel Jiang, Zixian Ma, Simran Khanuja, Ranjay Krishna, Graham Neubig, and Deva Ramanan. Naturalbench: Evaluating vision-language models on natural adversarial samples. *arXiv preprint arXiv:2410.14669*, 2024. 7

[46] Aniruddha Kembhavi, Mike Salvato, Eric Kolve, Minjoon Seo, Hannaneh Hajishirzi, and Ali Farhadi. A diagram is worth a dozen images. In *Computer Vision–ECCV 2016: 14th European Conference, Amsterdam, The Netherlands, October 11–14, 2016, Proceedings, Part IV 14*, pages 235–251. Springer, 2016. 7

[47] Ahmed Masry, Do Xuan Long, Jia Qing Tan, Shafiq Joty, and Enamul Hoque. Chartqa: A benchmark for question answering about charts with visual and logical reasoning. *arXiv preprint arXiv:2203.10244*, 2022. 7

[48] Minesh Mathew, Dimosthenis Karatzas, and CV Jawahar. Docvqa: A dataset for vqa on document images. In *Proceedings of the IEEE/CVF winter conference on applications of computer vision*, pages 2200–2209, 2021. 7

[49] Minesh Mathew, Viraj Bagal, Rubén Tito, Dimosthenis Karatzas, Ernest Valveny, and CV Jawahar. Infographicvqa. In *Proceedings of the IEEE/CVF Winter Conference on Applications of Computer Vision*, pages 1697–1706, 2022. 7

[50] x.ai. Introducing Grok 1.5v: The Latest Advancement in AI, November 2024. [Online; accessed 14-November-2024]. 7

[51] Ge Zhang, Xinrun Du, Bei Chen, Yiming Liang, Tongxu Luo, Tianyu Zheng, Kang Zhu, Yuyang Cheng, Chunpu Xu, Shuyue Guo, et al. Cmmmu: A chinese massive multi-discipline multimodal understanding benchmark. *arXiv preprint arXiv:2401.11944*, 2024. 7

Appendices

A. Computational complexity	12
A.1. Complexity analysis	12
A.2. Resource requirements	12
A.3. Discussion on cost-benefit justification	12
B. Additional experiment details & ablations	12
B.1. Additional task details	12
B.2. Projection dimension	12
B.3. Warm-up Ratio	12
C. Additional analysis	12
C.1. From specialist to generalist	12
C.2. Visual dependency influence ranking	14
C.3. Cross-architecture generalization	15
C.4. Consistency analysis	15
D. Algorithm details	15
E. Future work	16
F. Visualizations	16
F.1 . Representation-based vs. Gradient-based data selection	16
F.2 . Specialists & Generalist	17

A. Computational complexity

A.1. Complexity analysis

Computing gradient-based influence requires a non-trivial amount of computational resources. In the specialist stage, the complexity scales with both the dataset size $|\mathcal{D}|$ and the gradient dimension d . This stage consists of three steps. First, the warm-up training has a complexity of $\mathcal{O}(|\mathcal{D}_{\text{warmup}}|)$. Second, the gradient computation stage has a computational complexity of $\mathcal{O}(|\mathcal{D}| + |\mathcal{D}_{\text{val}}|)$ for forward and backward passes, with storage requirements of $\mathcal{O}(|\mathcal{D}| \cdot d + |\mathcal{D}_{\text{val}}| \cdot d)$ for the gradients. Third (and finally), the influence matrix computation requires $\mathcal{O}(|\mathcal{D}| \cdot |\mathcal{D}_{\text{val}}| \cdot d')$ compute cost, where d' is the reduced dimension after projection. The generalist stage, focusing on influence consensus across tasks, has lower computational requirements. It begins with threshold computation, requiring $\mathcal{O}(K \cdot |\mathcal{D}| \log |\mathcal{D}|)$ operations for sorting across K tasks. The voting process then takes $\mathcal{O}(K \cdot |\mathcal{D}|)$ compute, followed by a final selection step with complexity $\mathcal{O}(|\mathcal{D}| \log |\mathcal{D}|)$ for sorting the aggregated votes. Storage requirements for this stage are minimal, primarily for the final selected subset.

A.2. Resource requirements

In practice, for LLaVA-665K training data, the warmup training phase requires 0.75 hours using eight L40 GPUs. We parallelize the gradient computation across 100 A6000 GPUs, taking approximately one hour and requiring 103GB of total storage for the gradients. The influence consensus stage is notably efficient, completing in less than a minute on a single L40 GPU. While these computational demands are substantial, they represent front-loaded, one-time costs that can be used across multiple target tasks and model iterations. This makes our method extendable for new tasks, as the expensive training data gradient computations only need to be performed once.

A.3. Discussion on cost-benefit justification

Although gradient-based data selection is computationally intensive, we argue that the initial cost is justified by three key considerations. First, the computational expense is largely a one-time investment: once gradients are computed, they can be stored in our gradient datastore and reused across multiple model iterations, target tasks, and diverse downstream applications. This reusability becomes especially valuable as the number of target datasets grows, because each new target dataset can leverage existing gradient computations, making the selection increasingly efficient at scale.

Second, our empirical results demonstrate substantial performance benefits. Training on a strategically chosen 60% subset of data not only reduces training time but also surpasses the performance obtained by using the full dataset. This improvement underscores how directing more compute resources toward a carefully selected subset can yield higher returns on a fixed set of data.

Lastly, the initial compute-intensive investment in data selection is amortized across future training iterations and future developers. By leveraging the curated, higher-quality dataset, they can substantially reduce training costs.

B. Additional experiment details & ablations

We provide comprehensive experimental details and ablation studies to support our main findings. We first present detailed task descriptions and dataset statistics (Tab. 6), followed by detailed per-task results for aggregation method comparisons (Tab. 5) and full results for unseen benchmarks (Tab. 7). We then ablate key hyperparameters including projection dimension (§B.2) and warm-up ratio (§B.3).

B.1. Additional task details

Here, we provide further details on the target tasks, as summarized in Tab. 6. These tasks cover a wide range of multimodal benchmarks commonly used, including Yes/No questions (Y/N), multiple-choice understanding questions (MCQ) and visual question answering (VQA).

B.2. Projection dimension

We primarily set the projection dimension to 5120, reducing features from 338.7M to 5120 dimensions. The choice of 5120 was empirically validated for its trade-off between effectively capturing gradient representations and maintaining a manageable parameter space. Our LLaVA-v1.5-7b-lora architecture includes a total of 7.4B parameters, with 338.7M parameters being trainable after LoRA adaptation, accounting for approximately 4.58% of the total parameter count. We further ablate different projection dimensions (1024, 2560, 5120, and 10240), with results provided in Fig. 5a.

B.3. Warm-up Ratio

To initiate training, we use 5% of the total training data. We conducted ablation studies to evaluate the impact of varying warm-up ratios (5%, 10%, 20%, and 100%) on selection performance, as shown in Fig. 5b. Our experiments reveal that increasing the warm-up data size does not lead to performance improvements. Surprisingly, models trained with smaller warm-up ratios (5-20%) consistently outperform those trained with the full dataset (100%). Specifically, the 5% warm-up ratio achieves the best performance at 98.6%, while using the complete dataset results in a performance drop to 97.8%. This finding suggests that a small subset of training data is sufficient and even beneficial for model initialization, and potentially gives better signals in the early training stages.

C. Additional analysis

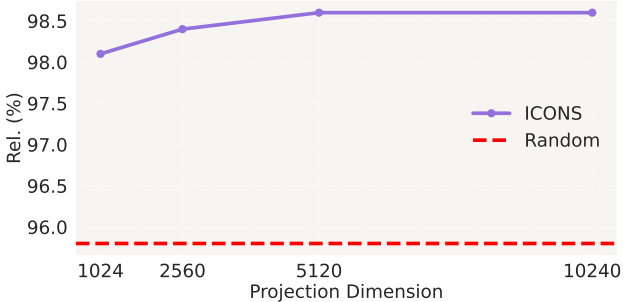
In this section, we provide additional analyses to better understand different aspects of our ICONS. We include detailed vote distribution visualizations (Fig. 6) extending the analysis from §4.6. We analyze the effectiveness of task-specific selections and their aggregation into a generalist subset (§C.1). We further explore whether incorporating visual dependency information into the selection process affects performance across different types of vision-language tasks (§C.2). We also evaluate the transferability of our selected subset across different model scales (§C.3). Additionally, we evaluate the consistency of our method across multiple runs (§C.4), showing its robustness and reliability.

C.1. From specialist to generalist

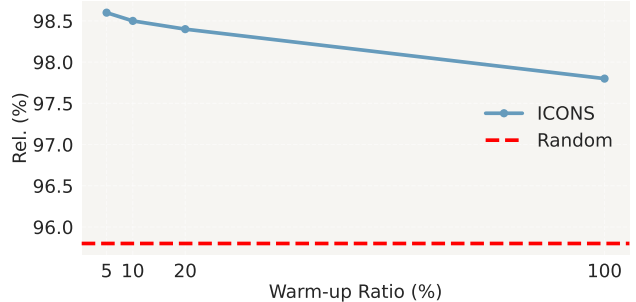
To understand the intermediate task-specific influence matrices we obtained from the specialist stage, we select 20% of data for

Table 5. **Detailed aggregation approaches comparison for Tab. 3.** Our proposed aggregation approach (**Vote**) consistently achieves the best overall performance (98.6% Rel.), outperforming both score-based (**Merge**, **Max**), their normalized variants (**Merge-GausNorm**, **Merge-SumNorm**) and rank-based (**Round Robin**, **MinRank**) baselines when selecting 20% of the LLAVA-665K dataset.

Aggregation	VQAv2	GQA	VizWiz	SQA-I	TextVQA	POPE	MME	MMB (en)	MMB (cn)	LLaVA-W	Rel. (%)
Full	79.1	63.0	47.8	68.4	58.2	86.4	1476.9	66.1	58.9	67.9	100
Merge	75.7	59.6	47.9	65.5	55.5	86.0	1422.1	59.0	51.0	66.2	96.4
Max	75.2	59.8	48.1	66.2	55.5	85.5	1470.7	58.3	51.8	66.2	96.1
Merge-GausNorm	75.1	60.1	46.4	69.8	54.5	85.6	1482.6	58.9	52.5	66.3	96.8
Merge-SumNorm	75.5	59.1	51.7	68.7	43.5	87.1	1478.3	59.5	50.9	69.8	95.3
Round Robin	75.4	59.1	48.3	70.6	55.2	86.6	1474.5	61.6	51.5	66.9	96.7
MinRank	75.2	59.0	49.7	70.4	55.1	86.9	1456.3	61.1	52.4	68.4	97.1
Vote (ours)	76.3	60.7	50.1	70.8	55.6	87.5	1485.7	63.1	55.8	66.1	98.6



(a) **Projection Dimension Ablation.** We show the performance of ICONS at different projected dimensions (1024, 2560, 5120, 10240), compared to the random baseline. The performance increases with the projected dimension and reaches a plateau around dimension 5120.



(b) **Warm-up Ratio Ablation.** The blue line represents ICONS performance across different warm-up ratios (5%, 10%, 20%, and 100%), while the red dashed line shows the random baseline performance. Results show that smaller warm-up ratios (5-20%) achieve better performance compared to using the full dataset (100%).

Figure 5. Ablation studies on (left) projection dimension and (right) warm-up ratio.

Table 6. **Statistics of Target Tasks.** Our target tasks include diverse benchmarks and answer formats, covering different vision-language capabilities. Task types include Multiple-Choice Questions (**MCQ**), Visual Question Answering (**VQA**), and Yes/No Questions (**Y/N**).

Task	MME	POPE	SQA-I	MMBench	
				en	cn
$ \mathcal{D}_{\text{val}} $	986	500	424	1,164	1,164
$ \mathcal{D}_{\text{test}} $	2,374	8,910	4,241	1,784	1,784
Task Type	Y/N	Y/N	MCQ	MCQ	MCQ
Task	VQAv2	GQA	VizWiz	TextVQA	LLaVA-W
$ \mathcal{D}_{\text{val}} $	1,000	398	800	84	84
$ \mathcal{D}_{\text{test}} $	36,807	12,578	8,000	5,000	84
Task Type	VQA	VQA	VQA	VQA	VQA

each individual task. The task-specific data (Specialists) achieves comparable or superior performance than full data training (Tab. 8). With influence consensus at the generalist stage, we select a 20% subset with only a 1.33% average drop across tasks compared to specialist baselines. This validates our approach: by understanding task-specific influence patterns and building consensus across tasks, we can identify a compact, universal training set that maintains strong performance with significantly less data.

Divergent multi-task influence patterns. As shown in Fig. 7, the

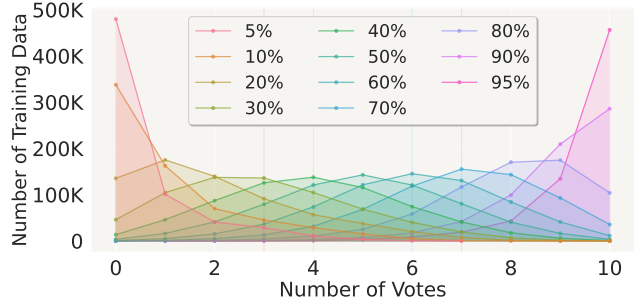


Figure 6. **Vote distributions across selection ratios.** Each line shows the vote distribution for a different selection ratio (5% to 95%). At lower ratios (e.g., 5%), most samples receive zero votes, resulting in a left-skewed distribution. As ratios increase (e.g., 50%, 70%, 90%), the distribution shifts rightward and flattens, with more samples receiving votes from multiple tasks. Stricter criteria (lower ratios) identify task-specific samples, while relaxed criteria (higher ratios) reveal broader multi-task agreement.

pairwise overlap heatmap shows notable variation in training data influence across tasks. High overlap – e.g., VQAv2 and VizWiz (49.0%) or POPE and GQA (60.2%), suggests that certain samples are beneficial across similar tasks. However, low overlap,

Table 7. **Detailed results of unseen task generalization.** Detailed results for Fig. 3. Performance comparison on unseen benchmarks when trained on selected 20% subsets. Notably, we observe improvements on InfoVQA (103.8%), RealWorldQA (104.4%), and CMMMU (114.0%), highlighting strong generalization to unseen tasks.

	AI2D	ChartQA	DocVQA	InfoVQA	MMVet	Naturalbench	RealworldQA	CMMMU	Rel. (%)
Full	55.4	17.5	28.9	26.5	31.1	12.4	52.4	22.1	100.0
Random	50.2	15.1	25.2	24.3	29.6	11.1	49.8	21.9	91.8
CLIP-Score	52.0	16.4	27.1	24.9	29.2	11.6	49.3	20.8	93.9
EL2N	52.1	17.9	26.9	26.4	29.6	12.5	51.9	21.7	97.8
Perplexity	53.0	16.4	27.1	27.1	29.4	11.4	50.3	23.9	97.0
SemDeDup	53.2	16.4	26.4	26.6	29.1	13.2	51.1	22.8	97.8
D2-Pruning	52.1	17.3	26.5	24.7	33.1	11.3	52.0	21.9	96.7
Self-Sup	52.7	16.6	27.4	25.2	29.6	11.8	50.1	21.0	95.0
Self-Filter	52.1	16.0	27.1	25.0	29.3	11.5	49.5	20.6	94.0
COINCIDE	53.7	17.0	27.9	26.0	30.2	12.1	50.9	21.4	97.2
RDS	53.0	16.8	27.5	25.4	29.8	12.0	50.3	21.3	95.6
LLAVA-ICONS-133K	53.9	17.1	27.9	27.5	29.7	12.8	55.0	25.2	101.6
Per-task Rel. (%)	97.3	97.7	96.5	103.8	95.5	103.2	104.4	114.0	-

Table 8. **Single-task Selection (Specialist) vs. Consensus-aware Multi-task Selection (Generalist).** The single-task data selection approach selects 20% of LLAVA-665K per task, while our consensus-aware multi-task data selection approach selects a total of 20% data across all tasks.

Method	VQAv2	GQA	VizWiz	SQA-I	TextVQA	POPE	MME	MMBench (en)	MMBench (cn)	LLaVA-W Bench
Full	79.1	63.0	47.8	68.4	58.2	86.4	1476.9	66.1	58.9	67.9
Specialist	77.1	61.1	53.1	69.8	55.7	86.6	1506.1	66.0	56.4	67.1
Generalist	76.3	60.7	50.1	70.8	55.6	87.5	1485.7	63.1	55.8	66.1
Delta (%)	1.04	0.65	5.65	-1.43	0.18	-1.04	1.35	4.34	1.06	1.49

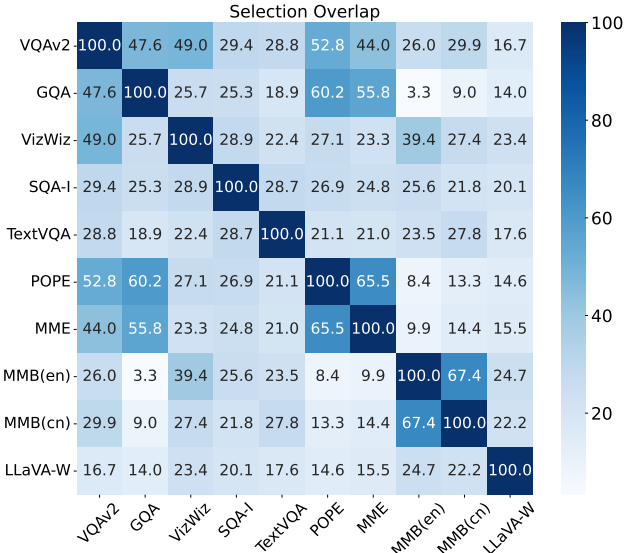


Figure 7. **Pairwise overlap heatmap between specialists.** The values show overlap percentages between benchmarks' selected samples.

like the 3.3% between MMBench (en) and GQA, highlights that highly influential samples for one task may have limited impact

on others. Even closely related tasks, such as MMBench in different languages (English and Chinese), share 67.4% of influential samples. To understand task-specific influence matrices from the specialist stage, we select the top 20% samples per task (Specialists). Overlap with our generalist subset (Fig. 8) varies significantly, from minimal in tasks like VQAv2 (3.27%) and VizWiz (3.28%) to substantial agreement in tasks like LLaVA-W Bench [2] (24.21%). These findings empirically demonstrate significant overlap in influential samples across tasks and validate our approach: by analyzing task-specific gradient-based influence patterns and building consensus across tasks, we can identify a compact subset that captures broadly useful samples across tasks, yielding strong performance with significantly less data.

C.2. Visual dependency influence ranking

Recent work [3] has shown that vision-language tasks vary in their reliance on visual information: tasks like MMBench [29] depend heavily on visual grounding, while others like SQA-I [35] can be handled primarily through language, showing only a 5% drop in performance when visual input is removed [3]. To take visual dependency of training data into account, we further explored gradient-based Visual Dependency Score (**VDS**). For each data point, we calculate the gradient of the model's auto-regressive cross-entropy loss with both the original image and a Gaussian noise image $I_{\text{noise}} \sim \mathcal{N}(0, 1)$, keeping the text input constant. This quantifies how much the visual component contributes to model performance. We construct an adapted influence matrix: visual

	VQAv2	GQA	VizWiz	SQA-I	TextVQA	POPE	MME	MMBench (en)	MMBench (cn)	LLaVA-W Bench
Full	79.1	63.0	47.8	68.4	58.2	86.4	1476.9	66.1	58.9	67.9
w/o VDS	76.3	60.7	50.1	70.8	55.6	87.5	1485.7	63.1	55.8	66.1
w/ VDS	75.8	60.9	50.3	69.5	54.8	86.8	1489.3	64.3	56.3	67.9
Delta (%)	-0.66	+0.33	+0.40	-1.84	-1.44	-0.80	+0.24	+1.90	+0.90	+2.72

Table 9. **Impact of Visual Dependency Score (VDS) on Selection Performance.** Rows show performance without VDS, with VDS, and the performance change (Delta). VDS improves performance on LLaVA-W Bench (+2.72%), MMBench (en) (+1.90%), and MMBench (cn) (+0.90%), but decreases performance on SQA-I (-1.84%), TextVQA (-1.44%), and POPE (-0.80%).

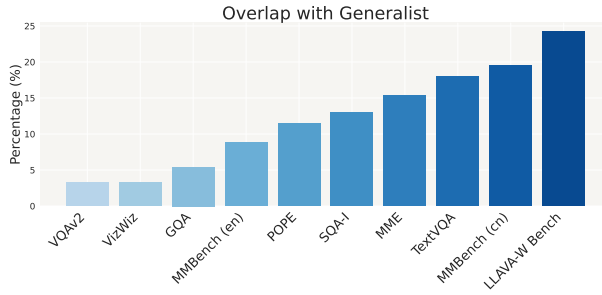


Figure 8. **Data overlap between specialists and generalist selection.** Overlap varies significantly, from 3.27% (VQAv2) to 24.21% (LLaVA-W Bench), reflecting varying alignment between task-specific and consensus selections.

influence matrix $\mathcal{I}_{\text{VDS}} \in \mathbb{R}^{|\mathcal{D}| \times |\mathcal{D}_{\text{val}}|}$, which quantifies the visual influence of each training sample \mathbf{z}_i on each validation sample \mathbf{z}'_j w.r.t the model’s gradient alignment and visual dependency. \mathcal{I}_{VDS} is computed as:

$$\mathcal{I}_{\text{VDS},ij} = \langle \nabla_{\theta} \mathcal{L}(\mathbf{z}'_i), \nabla_{\theta} \mathcal{L}(\mathbf{x}_j, I_j) - \nabla_{\theta} \mathcal{L}(\mathbf{x}_j, I_{\text{noise}}) \rangle, \quad (9)$$

where $\nabla_{\theta} \mathcal{L}(\mathbf{x}_j, I_j)$ and $\nabla_{\theta} \mathcal{L}(\mathbf{x}_j, I_{\text{noise}})$ are the gradients computed with the original and Gaussian noise images, respectively. The visual influence matrix \mathcal{I}_{VDS} provides insights into which training samples have the most influence on the validation samples from a visual perspective. This matrix can be used to further rank and select training data that are most impactful for tasks requiring strong visual grounding, ensuring that the selected subset effectively supports vision-dependent performance.

Our empirical results demonstrate that VDS-based data selection has varying effectiveness across different tasks (Tab. 9). It shows substantial improvements on tasks requiring strong visual understanding, such as open-ended generation (LLaVA-W Bench: +2.72%) and multiple-choice understanding (MMBench-EN: +1.90%, MMBench-CN: +0.90%). However, tasks that primarily rely on textual reasoning show decreased performance, including SQA-I (-1.84%) and TextVQA (-1.44%). These results align with and extend the findings in Cambrian [3], demonstrating that the effectiveness of VDS corresponds to a task’s visual dependency - tasks that maintain performance without visual inputs show limited or negative impact from VDS-based selection, while visually-dependent tasks benefit significantly. This pattern suggests that VDS effectively identifies training samples where visual information plays an important role in training.

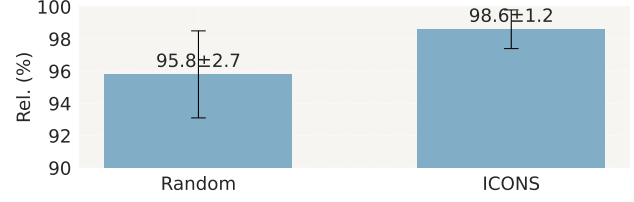


Figure 9. **Rel. (%) Across Runs.** We show the performance across three different runs for random selection and our ICONS.

C.3. Cross-architecture generalization

We conduct experiments on cross architecture generalization to evaluate the transferability of our selected data across different model scales. While our subset was initially selected using LLaVA-v1.5-7B as the base model, we investigate whether these same examples remain effective for training larger architectures like LLaVA-v1.5-13B. This tests whether our selection criteria identify universally valuable training examples rather than model-specific patterns. Our results in Tab. 10 show cross-architecture generalization, with 13B model trained on 7B-selected subset achieving 98.1% Rel.. Both 7B-selected and 13B-selected subsets outperform random selection (95.7%), with the 13B-selected option showing particular strength in reasoning tasks like MMBench and POPE. This suggests our selected subset captures fundamental visual-language understanding patterns that generalize well across different model architectures.

C.4. Consistency analysis

To evaluate the consistency of ICONS, we conduct three independent runs of the experiments. As shown in Fig. 9, our method demonstrates high consistency across different runs, achieving $98.6 \pm 1.2\%$ Rel., which shows a notable improvement over random baseline, which achieves $95.8 \pm 2.7\%$. The lower standard deviation (1.2% vs 2.7%) further indicates that our approach produces more stable and reliable outcomes compared to the random baseline.

D. Algorithm details

We provide detailed pseudocode for our two-stage ICONS framework. Stage 1 (specialist) computes task-specific influence scores through gradient-based analysis with efficient random projections. Stage 2 (generalist) implements our voting-based consensus mechanism to select samples that are influential across multiple tasks.

Table 10. **Cross-Architecture Generalization.** Our LLAVA-ICONS-133K selected via LLAVA-v1.5-7B model (7B-selected) shows strong cross-architecture transferability, achieving 97.3% Rel., while the data selected via LLAVA-v1.5-13B model (13B-selected) reaches 98.1%, showing that our selected subset generalizes well to different architectures.

	VQAv2	GQA	Vizwiz	SQA-I	TextVQA	POPE	MME	MMBench (en)	MMBench (cn)	LLAVA-W	Rel. (%)
Full	80.0	63.3	58.9	71.2	60.2	86.7	1541.7	68.5	61.5	69.5	100.0
Random	77.3	60.7	57.6	69.1	56.8	82.9	1517.2	63.2	56.3	67.5	95.7
7B-selected	78.8	60.4	57.4	70.4	58.3	84.3	1527.5	64.9	59.7	68.2	97.3
13B-selected	78.9	61.2	57.5	71.3	58.4	85.9	1535.2	66.1	59.8	68.8	98.1

Algorithm 1 ICONS Stage 1: Specialist (Task-specific Influence Computation)

```

Require: Training dataset  $D = \{(x_i, I_i, y_i)\}_{i=1}^N$ , target tasks  $T = \{T_1, \dots, T_K\}$ 
Require: Warm-up ratio  $r$  (default 5%)
Ensure: Task-specific influence scores  $\{\bar{I}_k\}_{k=1}^K$ 
1: for each task  $T_k \in T$  do
2:   // Step 1: Warm-up Training
3:   Sample warm-up set  $D_{\text{warmup}} \subset D$  of size  $r|D|$ 
4:    $f_{\text{warmup}} \leftarrow \text{LoRA}(f_{\text{base}}, D_{\text{warmup}})$ 
5:   // Step 2: Gradient Computation
6:   for each training sample  $z_i \in D$  do
7:      $g_i \leftarrow \nabla_{\theta_w} L(f_{\text{warmup}}(z_i), y_i)$ 
8:      $\tilde{g}_i \leftarrow \text{Normalize}(Rg_i)$  {Random projection}
9:   for each validation data  $z'_j \in D_{\text{val}}^k$  do
10:     $g'_j \leftarrow \nabla_{\theta_w} L(f_{\text{warmup}}(z'_j), y'_j)$ 
11:     $\tilde{g}'_j \leftarrow \text{Normalize}(Rg'_j)$ 
12:   // Step 3: Influence Matrix Computation
13:   for each  $z_i \in D, z'_j \in D_{\text{val}}^k$  do
14:      $I_{ij}^k \leftarrow \langle \tilde{g}_i, \tilde{g}'_j \rangle$ 
15:   // Compute average influence per training sample
16:    $\bar{I}_k(z_i) \leftarrow \frac{1}{|D_{\text{val}}^k|} \sum_{j=1}^{|D_{\text{val}}^k|} I_{ij}^k$ 
17: return Task-specific influence scores  $\{\bar{I}_k\}_{k=1}^K$ 

```

E. Future work

Our work opens several promising research directions for improving vision-language data selection. While our work focuses specifically on visual instruction tuning data, our influence consensus approach can be naturally extended to other stages of MLLM training, such as alignment stage. The majority voting mechanism may under-represent tasks with unique characteristics or those in the long tail, as it prioritizes samples that broadly benefit multiple tasks to build the *main knowledge pool*. This can lead to limited support for specialized tasks or the reinforcement of spurious correlations spanning multiple tasks. Future work could explore **weighted voting mechanisms**, in which tasks are assigned weights based on their relative importance or contribution to overall model performance for more balanced data selection. Additionally, investigating more efficient gradient computation and storage methods would help scale these methods to larger datasets while maintaining strong

Algorithm 2 ICONS Stage 2: Generalist (Influence Consensus-based Data Selection)

```

Require: Task-specific influence scores  $\{\bar{I}_k\}_{k=1}^K$ 
Require: Selection ratio  $p$ , number of tasks  $K$ 
Ensure: Selected subset  $S \subset D$  of size  $m \ll N$ 
1: // Compute voting thresholds
2: for each task  $T_k \in T$  do
3:    $\tau_k \leftarrow (1 - p)$ -th percentile of  $\{\bar{I}_k(z_i)\}_{i=1}^N$ 
4: // Voting process
5: for each training sample  $z_i \in D$  do
6:    $I_{\text{vote}}(z_i) \leftarrow 0$ 
7:   for each task  $T_k \in T$  do
8:      $\text{vote}_k(z_i) \leftarrow \mathbb{1}[\bar{I}_k(z_i) \geq \tau_k]$ 
9:      $I_{\text{vote}}(z_i) \leftarrow I_{\text{vote}}(z_i) + \text{vote}_k(z_i)$ 
10: // Select top samples based on total votes
11:  $S \leftarrow \text{top-}p$  samples by  $I_{\text{vote}}$ 
12: return Selected subset  $S$ 

```

performance across diverse vision-language tasks.

F. Visualizations

In this section, we provide detailed visualizations. We compare representation-based versus gradient-based data selection approaches (§F.1), showing qualitative differences in selected samples, and visualize the most influential examples identified by both task-specific specialists and the generalist model across all target tasks (§F.2). Additionally, we present examples of low-vote training samples (Fig. 10), which are referenced in §4.7 of the main paper, to illustrate the characteristics of data filtered out by our method.

F.1. Representation-based vs. Gradient-based data selection

While ICONS leverages gradient-based influence signals, we explore how representation-based data selection (RDS) performs in the same setting (§4.2). We compare the top-ranked training samples selected after the generalist stage by RDS with those selected by ICONS in Fig. 22. Interestingly, we observe that the representation-based variants often favor training examples with repeated images or instructions, which may dominate the learned representations without contributing to better generalization. Some of the highest-scoring samples under representation-based similarity are duplicated image-question pairs with only the answer

choices shuffled. We hypothesize that this is a side effect of the way multimodal representations are constructed, where visually dominant or textually redundant samples occupy high-density regions in embedding space. However, these samples do not necessarily translate into broader utility across tasks, as seen in the performance gap in Tab. 1. This discrepancy raises broader questions about what it means for multimodal data to be *diverse*. While we leave these questions open for future exploration, our results suggest that gradient-based influence, though computationally more expensive, is better aligned with generalization and multi-task data mixture settings.

F.2. Specialists & Generalist

We visualize the most influential top three examples across specialists (Figs. 12 to 21) and the generalist selection (Fig. 22), along with samples from their corresponding tasks. Notably, the selected high-influence examples by specialists show strong task-specific characteristics both structurally and contextually - they mirror the key attributes of their target tasks in terms of question structure, reasoning patterns, and required visual-language understanding capabilities. Furthermore, the visualization of top influential examples reveals distinct patterns in what makes training samples valuable for different vision-language tasks. VQAv2, GQA, and SQA-I specialists favor multi-turn Q&A scenarios that test both visual comprehension and contextual understanding, while TextVQA, POPE, and MME specialists emphasize text recognition, object verification, and spatial relationships respectively. MMBench-EN and MMBench-CN show consistent patterns despite language differences, focusing on clear, unambiguous scenes that translate well. The LLaVA-W Bench specialist prioritizes examples requiring detailed explanations and multi-step reasoning, and the answers are generally longer. The generalist model values diverse scenarios that combine multiple skills simultaneously. Common characteristics that make these examples particularly valuable include multi-turn interactions, clear visual elements, factual and inferential reasoning, cross-modal interaction, and the ability to test multiple capabilities within a single example. This suggests that the most effective training samples are those that combine multiple types of reasoning while maintaining clear, unambiguous ground truth that can be consistently learned across tasks.

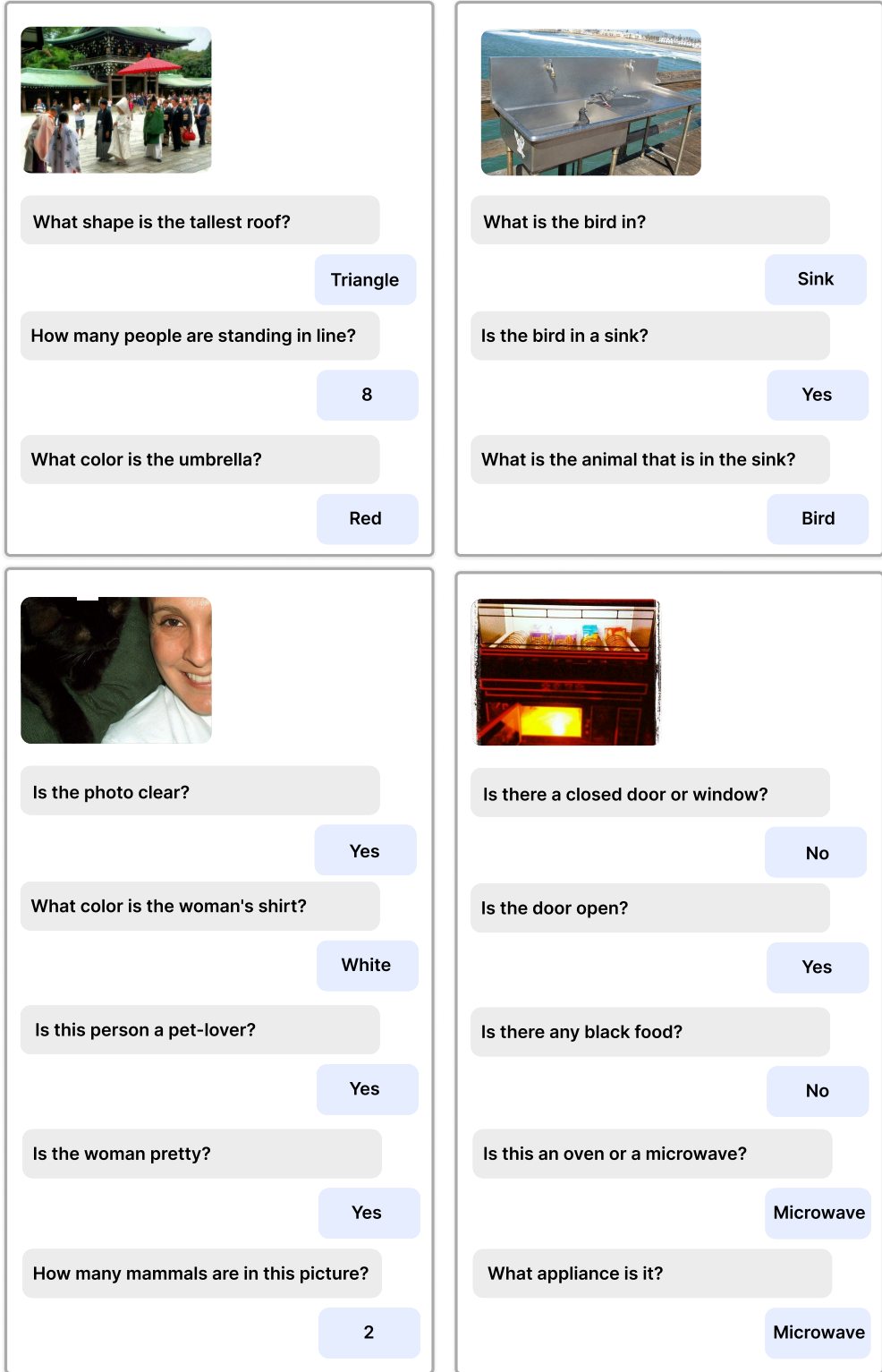


Figure 10. **Examples of 0 & 1-vote training samples.** These low-vote samples exhibit characteristics that explain their low selection frequency: (1) subjective questions lacking objective ground truth (e.g., “Is the woman pretty?”), (2) trivial questions providing minimal visual learning signal (e.g., “Is the door open?”), (3) redundant questions about the same image content. By filtering out such potentially harmful or redundant examples, ICONS focuses training on more informative and generalizable samples.



What are the floating blue objects for?

- A. swimming
- B. boundaries
- C. decoration
- D. first aid

Answer with the option's letter from the given choices directly

B



Please provide a short description for this region: [0.0, 0.33, 0.83, 0.55]

Right side of pizza

Please provide a short description for this region: [0.02, 0.42, 0.48, 0.55].

Piece of pizza closest to brown plate at bottom

Please provide the bounding box coordinate of the region this sentence describes: a margarita pizza

[0.0, 0.33, 0.83, 0.55]



What are the floating blue objects for?

- A. decoration
- B. first aid
- C. swimming
- D. boundaries

Answer with the option's letter from the given choices directly

D

Please provide the bounding box coordinate of the region this sentence describes: far edge of pizza

[0.0, 0.33, 0.83, 0.55]

Please provide the bounding box coordinate of the region this sentence describes: pizza

[0.0, 0.33, 0.83, 0.55]

Please provide a short description for this region: [0.0, 0.33, 0.83, 0.55].

Pizza area on the right side of the plate

Please provide a short description for this region: [0.02, 0.42, 0.48, 0.55].

Closest slice with only a little tomato.

Figure 11. **Top three samples selected by RDS.** These highly-ranked samples are selected due to representation-based similarity but do not necessarily contribute to better generalization, highlighting a key limitation of representation-based selection in multimodal settings.

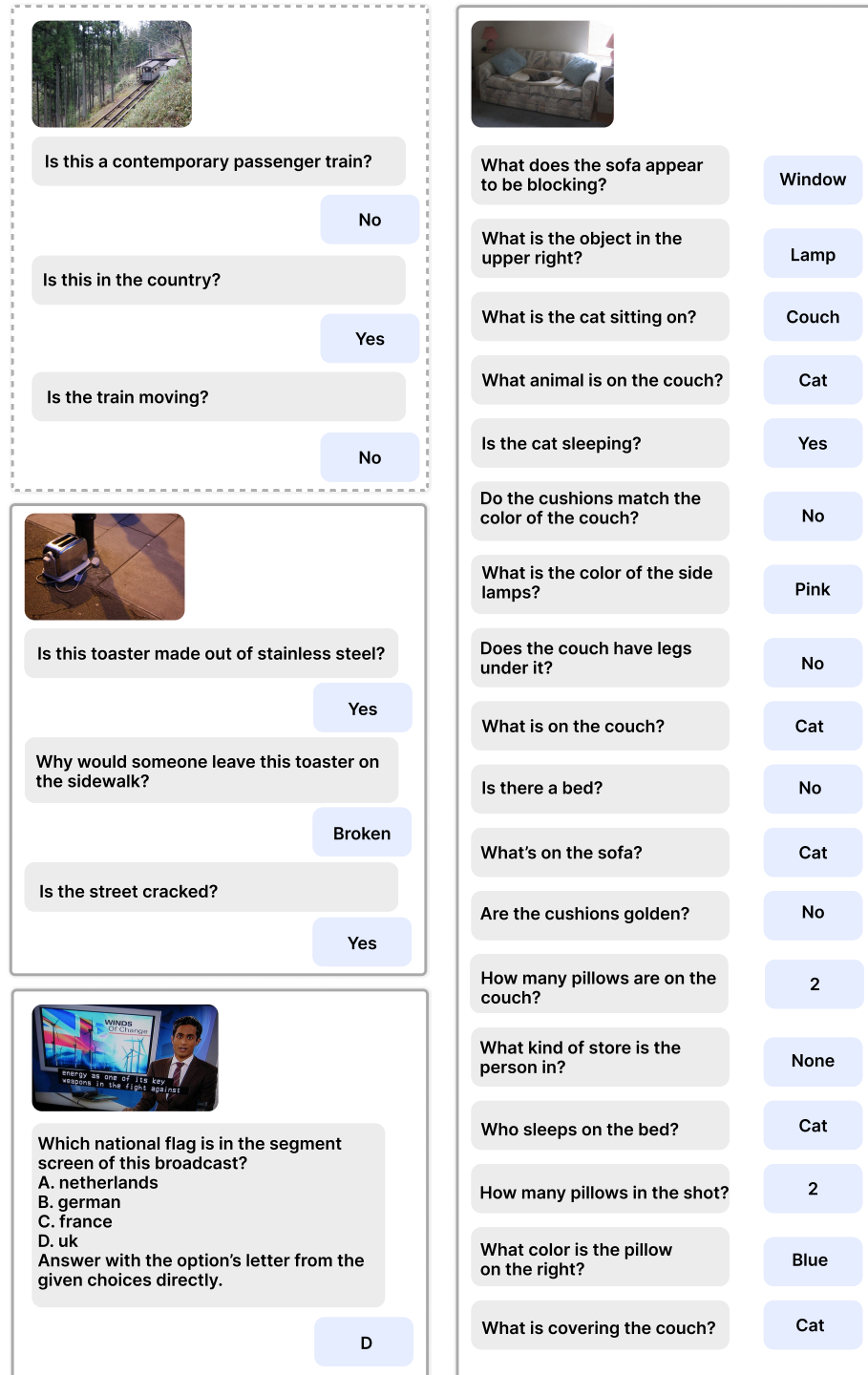


Figure 12. **VQAv2**. Top-left: A sample from VQAv2 [31]. Remaining panels show top three influential samples selected using the specialist influence ranking step.

 <p>Is it overcast?</p> <p>No</p> <p>Do you see both helmets and skis?</p> <p>No</p> <p>Are the snow pants green?</p> <p>Yes</p> <p>Is the snow both bright and white?</p> <p>Yes</p> <p>Is there either a fence or a snowboard in the photograph?</p> <p>Yes</p> <p>What is the person in front of?</p> <p>Sky</p> <p>What's the person in front of?</p> <p>Sky</p> <p>What is the person doing?</p> <p>Snowboarding</p> <p>What is the person in front of the sky doing?</p> <p>Snowboarding</p> <p>How hard is the snowboard?</p> <p>Very</p> <p>Do the number and the shirt have the same color?</p> <p>Yes</p> <p>Does the snowboard look red and hard?</p> <p>Yes</p> <p>Are there red snowboards or kites?</p> <p>Yes</p>	 <p>Please provide the bounding box coordinate of the region this sentence describes: a large rock in back.</p> <p>[0.31, 0.08, 0.49, 0.35]</p> <p>Please provide the bounding box coordinate of the region this sentence describes: black stripes on zebra fur.</p> <p>[0.43, 0.37, 0.58, 0.42]</p> <p>Please provide a short description for this region: [0.33, 0.32, 0.63, 0.58].</p> <p>A small zebra with big black stripes.</p> <p>Please provide a short description for this region: [0.33, 0.11, 0.48, 0.34].</p> <p>Rock structure in grass.</p> <p>Please provide a short description for this region: [0.67, 0.76, 0.76, 0.84].</p> <p>Black zebra hooves.</p> <p>Please provide the bounding box coordinate of the region this sentence describes: the zebra is eating grass.</p> <p>[0.31, 0.44, 0.42, 0.58]</p> <p>Please provide the bounding box coordinate of the region this sentence describes: a zebra having a snack.</p> <p>[0.65, 0.54, 0.81, 0.85]</p> <p>Please provide a short description for this region: [0.61, 0.77, 0.79, 0.86].</p> <p>A zebra shadow in grass.</p> <p>Please provide a short description for this region: [0.31, 0.32, 0.66, 0.58].</p> <p>An animal standing in place.</p> <p>Please provide the bounding box coordinate of the region this sentence describes: a striped zebra eating.</p> <p>[0.33, 0.32, 0.63, 0.57]</p>	 <p>Who is the catcher in front of?</p> <p>Men</p> <p>Who is in front of the men that are wearing a helmet?</p> <p>Catcher</p> <p>Who is wearing a uniform?</p> <p>Men</p> <p>Are the men to the left of the catcher wearing a cap?</p> <p>No</p> <p>Who is wearing a helmet?</p> <p>Men</p> <p>Who wears the face mask?</p> <p>Men</p> <p>Who is wearing helmets?</p> <p>Catcher</p> <p>What kind of clothing is black?</p> <p>Uniform</p> <p>Are the trousers white?</p> <p>Yes</p> <p>Who wears a face mask?</p> <p>Men</p> <p>Do the number and the shirt have the same color?</p> <p>Yes</p> <p>Which place is it?</p> <p>Stadium</p> <p>What place was the image taken at?</p> <p>Stadium</p> <p>What is the person in front of the men wearing?</p> <p>Helmets</p> <p>Does that uniform look blue?</p> <p>No</p> <p>What is the catcher wearing?</p> <p>Helmets</p> <p>Which color is the shirt?</p> <p>White</p> <p>What is the black clothing item called?</p> <p>Uniform</p> <p>Is the color of the uniform different than the belt?</p> <p>No</p> <p>Who is wearing the uniform?</p> <p>Men</p>
 <p>Which place is it?</p> <p>Airport</p> <p>On which side is the man?</p> <p>Left</p>	<p>Please provide a short description for this region: [0.31, 0.32, 0.66, 0.58].</p> <p>An animal standing in place.</p> <p>[0.33, 0.32, 0.63, 0.57]</p>	

Figure 13. **GQA**. Top-left: A sample from GQA [32]. Remaining panels show top three influential samples selected using the specialist influence ranking step.



What is this? and what color is it?
When the provided information is insufficient, respond with 'Unanswerable'.
Answer the question using a single word or phrase.

Black



Would this be a good entree?

No

What is the white cloth that those snacks are sitting on

Doily

Would this be an appropriate food to serve to an infant?

No



What are the people holding in their hands?

Food

Is this a teddy bear?

No

Is the girl feeding the elephant?

No

Why are these people gathered together?

Zoo

Is this some kind of celebration?

No

Are there flowers on the girl's dress?

Yes

Is this someone's home?

No

Where are the people in the picture?

Zoo

Was this photo taken in a zoo?

Yes

Is the sky clear?

Yes

Is it summertime?

Yes



Is this a man?

No

Is there a parking lot?

Yes

Does this person look upset?

No

Is the lady going up or down the mountain?

Down

Figure 14. **VizWiz**. Top-left: A sample from VizWiz [33]. Remaining panels show top three influential samples selected using the specialist influence ranking step.



Context: Select the best answer. Which property do these three objects have in common?

A. shiny
B. slippery
C. opaque

C



Are there pipes in the bathroom?

Yes

What kind of floor is in the photo?

Black

What is color of the toilet seat?

White

Is the toilet functional?

Yes



How many stools are next to the kitchen counter or island?

There are two stools next to the kitchen counter or island.

What color is the refrigerator in the kitchen?

The refrigerator in the kitchen is white.

What type of material is used for the table and chairs?

The table and chairs are made of wood.

Can you describe the layout of the living space and kitchen?

The living space and kitchen have an open floor plan, which means they are situated next to each other without any wall separations or partitions. This design creates a spacious, airy, and connected environment that allows for easy socialization and movement between the two spaces. In the kitchen, there is a small island with two stools near it, providing a casual seating area for dining or conversation. The wooden table and chairs, along with the white refrigerator, further contribute to the overall aesthetic and layout of the combined living and kitchen area.



What is Santa using?

Laptop

What is the Santa doing?

Typing

Could it be Christmas?

Yes

Is this indoors?

Yes

Figure 15. SQA. Top-left: A sample from SQA [35]. Remaining panels show top three influential samples selected using the specialist influence ranking step.



What is the brand of this camera?

Dakota digital



The man wearing the suit and tie is operating what object?

A. sedan
B. coupe
C. pickup truck
D. suv

Answer with the option's letter from the given choices directly.

C



Please provide a short description for this region: [0.21, 0.4, 0.41, 0.74]

Bird biggest.



Please provide the bounding box coordinate of the region this sentence describes: man in a brown tshirt.

[0.21, 0.31, 0.34, 0.76]

Please provide a short description for this region: [0.31, 0.32, 0.48, 0.73].

This is a man wearing a blue shirt, reaching to shake hands with his team mate.

[0.66, 0.36, 0.81, 0.78]

Please provide the bounding box coordinate of the region this sentence describes: man standing with raquet in white shirt on near side of net.

[0.31, 0.32, 0.48, 0.73]

Please provide the bounding box coordinate of the region this sentence describes: smiling black dude congratulates the winners of a tennis game.

A man with a white outfit and a tennis racket with blue handle.

A man in a brown shirt.

[0.53, 0.35, 0.71, 0.73]

Please provide a short description for this region: [0.21, 0.31, 0.34, 0.76].

Please provide the bounding box coordinate of the region this sentence describes: a man in a white shirt holding his hand out.

Please provide the bounding box coordinate of the region this sentence describes: the bald older white man playing tennis.

[0.53, 0.35, 0.71, 0.73]

Figure 16. **TextVQA**. Top-left: A sample from TextVQA [34]. Remaining panels show top three influential samples selected using the specialist influence ranking step.



Is there a baseball glove in the image?
Answer the question using a single word or phrase.

No

Is there a dog in the image?

Is there a person in the image?

Is there a car in the image?

Is there a sports ball in the image?

Is there a tennis racket in the image?

Is there a baseball glove in the image?

Is there a cake in the image?

Is there a refrigerator in the image?

Is there a sports ball in the image?

Is there a cat in the image?

Is there a baseball glove in the image?

Is there a dining table in the image?

Is there a sports ball in the image?

Is there a cup in the image?



What shape is the dogs tag?
Answer the question using a single word or phrase.

Bone

What kind of dog is this?

Beagle

What is the dog looking in?

Mirror



On which side of the picture is the white dog?
Answer the question using a single word or phrase.

Left

Do you see any dogs or cats there?

Yes

What is under the counter top?

Drawers

What is under the countertop?

Drawers

What kind of furniture is under the counter top?

Drawers

What kind of furniture is under the countertop?

Drawers

Is there a white dog or cat?

Yes

Are there both cabinets and bowls in the picture?

No

Does the trash can look large and white?

No

How large is the trashcan on the left side?

Small

Does the garbage can have a different color than the dog?

No

What animal has the same color as the small trash can?

Dog

Are there any ovens or bowls in the photo?

No

Which side of the image are the drawers on, the right or the left?

Right

What animal is it?

Dog

Figure 17. **Pope**. Top-left: A sample from Pope [36]. Remaining panels show top three influential samples selected using the specialist influence ranking step.

```

x = 10
if x < 20:
    print("Hello")
else:
    print("World")

```

The image shows a python code. Is the output of the code 'Hello'? Please answer yes or no.

Yes

The image shows a python code. Is the output of the code 'World'? Please answer yes or no.

No



Please provide the bounding box coordinate of the region this sentence describes: a large rock in back.

[0.31, 0.08, 0.49, 0.35]

Please provide the bounding box coordinate of the region this sentence describes: black stripes on zebra fur.

[0.43, 0.37, 0.58, 0.42]

Please provide a short description for this region: [0.33, 0.32, 0.63, 0.58].

A small zebra with big black stripes.

Please provide a short description for this region: [0.33, 0.11, 0.48, 0.34].

Rock structure in grass.

Please provide a short description for this region: [0.67, 0.76, 0.76, 0.84].

Black zebra hooves.

Please provide the bounding box coordinate of the region this sentence describes: the zebra is eating grass.

[0.31, 0.44, 0.42, 0.58]

Please provide the bounding box coordinate of the region this sentence describes: a zebra having a snack.

[0.65, 0.54, 0.81, 0.85]

Please provide a short description for this region: [0.61, 0.77, 0.79, 0.86].

A zebra shadow in grass.

Please provide a short description for this region: [0.31, 0.32, 0.66, 0.58].

An animal standing in place.

Please provide the bounding box coordinate of the region this sentence describes: a striped zebra eating.

[0.33, 0.32, 0.63, 0.57]

Figure 18. **MME**. Top-left: A sample from MME [30]. Remaining panels show top three influential samples selected using the specialist influence ranking step.

[Back to Table of Contents](#)

26

[Back to the First Page](#)



Question: Which of the following was a dependent variable in this experiment?

A: the temperature of the soda
B: the size of the ice pieces

A



Why is the man midair in the middle of the steps?

A. was thrown
B. he fell
C. stood up
D. performing trick

Answer with the option's letter from the given choices directly.

D



Is the machine turned on?
Answer the question using a single word or phrase.

Yes



What type of bread is this?
Answer the question using a single word or phrase.

Banana

Where is this machine used?

Kitchen

Can you see through the bottle on the right?

Yes

Figure 19. **MMBench (en)**. Top-left: A sample from MMBench (en) [29]. Remaining panels show top three influential samples selected using the specialist influence ranking step.



Question: 这两个物体有什么共同的属性？

A: 黄色
B: 咸的

B



Is the machine turned on?
Answer the question using a single word or phrase.

Yes

Where is this machine used?

Kitchen

Can you see through the bottle on the right?

Yes



Is the window open?
Answer the question using a single word or phrase.

Yes

Could the bed's metal leg be broken?

No

What color are the blinds/shutters?

White

What is seen in the room?

Bed

What kind of tree is closest to the house?

Oak

What is the blue object?

Bed



Why is the man midair in the middle of the steps?

A. was thrown
B. he fell
C. stood up
D. performing trick

Answer with the option's letter from the given choices directly.

D

Figure 20. **MMBench (cn)**. Top-left: A sample from MMBench (cn) [29]. Remaining panels show top three influential samples selected using the specialist influence ranking step.



What type of fruit is this?

This is a mangosteen fruit.

How many uncut fruits are in the image?

There are three uncut fruits in the image.

Describe this photo in detail.

This photo features four mangosteens on a wooden table. Three of them are uncut, showing their round, dark purple exterior. The fourth mangosteen is cut open, revealing its white, fleshy interior, which is divided into segments. The table surface has a natural wood grain pattern and adds a rustic touch to the image.

Imagine the fragrance of the fruits in the image. How would you describe this to someone who has never had this fruit before?

The fragrance of the mangosteens in the image can be described as sweet and slightly floral, with a hint of citrus aroma. It is a delicate and pleasant smell that entices you to try the fruit.



Who is in the image?

In the image, there is a person wearing skis and a dog, both out in the snow.

Based on the image, what activity is the person likely about to engage in?

Based on the image, the person is likely about to engage in skiing with their dog.

What is the context of the photo? Where is it likely taken?

The context of the photo is that it is being taken outside a ski patrol building. The skier and their dog are likely in a ski resort or mountainous area suitable for skiing.

Could the skier be part of the ski patrol team?

It is possible that the skier could be part of the ski patrol team, especially since they are posing outside of a ski patrol building. However, there isn't enough information in the image to say for certain whether they are a ski patrol official.

How could a dog participate or contribute to skiing activities?

Dogs can participate in skiing activities in several ways, often as companions or support animals. Some common ways dogs join skiing activities are:

- Skijoring: In this winter sport, a person on skis is pulled by a dog (or a team of dogs) on a harness. Skijoring combines aspects of cross-country skiing and dog sledding, and both the dog and the skier work together to navigate snowy trails.
- Ski patrol dogs: Ski patrol teams may have dogs trained for search and rescue missions, avalanche response, and providing comfort to injured skiers. These dogs are typically of large breeds like German Shepherds, Golden Retrievers, or Labrador Retrievers, and are specifically trained to handle challenging winter conditions.
- Companion dogs: Many dog owners bring their dogs along for recreational cross-country or backcountry skiing. These dogs do not necessarily have formal training but are physically capable of handling cold temperatures and snowy terrain, and they accompany their owners as companions on the trails.

In the image provided, it's unclear what specific role the dog may play or how they will participate in the skiing activity. However, it's evident that the dog will accompany the skier during their skiing session.



What are the key elements in this picture?

The image features a city street where a long row of parked motorcycles and mopeds are lined up along the sidewalk. There are several motorcycles of various sizes and designs, creating a neat row that extends across the side of the street.

There is also a notable presence of pedestrians in the area, as numerous people can be seen walking around and engaging in different activities. A backpack is located close to one of the people, placed on the pavement.

In addition to the motorcycles, other vehicles are present on the street, including a car and a truck parked near the sidewalk, adding to the urban scene's atmosphere.

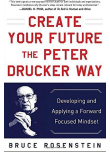


Why might passengers need to pay attention to the surroundings at the train station?

At the train station, passengers should be alert to their surroundings for various reasons. In the image, a train is moving along the tracks, and a green light indicates that it is safe to proceed. However, there are several elements to be aware of in the scene, such as other people near the tracks, cars nearby, and potential transit-related changes signaled by the traffic lights. Being attentive to the surroundings can help people anticipate changes in train schedules, ensure they board the correct train, and avoid accidents or other safety hazards.

Additionally, it is essential to be mindful of fellow travelers' presence and maintain a safe distance from the tracks to ensure both personal safety and the well-being of others. This can help create a safe and efficient environment at the train station for everyone.

Figure 21. **LLaVA-W Bench**. Top-left: A sample from LLaVA-W Bench [2]. Remaining panels show top three influential samples selected using the specialist influence ranking step.



Who is the author of this book?

Bruce Rosenstein

What is the title of this book?

Create Your Future the Peter Drucker Way:
Developing and Applying a Forward-Focused Mindset

What type of book is this?

Business & Money

Is this a financial book?

Yes

Is this a kids book?

No



What precautions should these young adults take to ensure safety while playing the Wii game?

To ensure safety while playing the Wii game, these young adults should maintain an adequate distance from each other, the TV, and other objects in the room. With the use of the Wii remotes, they should have sufficient space for movement to prevent accidentally hitting or running into each other, furniture, or nearby items. Furthermore, they should consider using wrist straps for the remotes to reduce the risk of accidentally throwing the controller during gameplay. Finally, keeping the play area clean and free from obstructions, such as loose cables or objects on the floor, can help minimize the risk of trip hazards and improve safety.



What could be a possible use case for the items on the desk?

A possible use case for the items on the desk is a home office or a gaming setup. The desk has a computer monitor, keyboard, mouse, and a headset, which indicates that it is a workstation that could be used for tasks requiring a personal computer. These tasks could involve remote work, video editing, software development, or other professional activities. In addition, the presence of the headset and the gaming peripherals such as the mouse and keyboard can also suggest a gaming setup, where the person uses their computer for playing video games, communicating with other players using the headset, or even streaming their gameplay online. The desk might also be used for general computer use, such as browsing the internet, watching movies, or using social media platforms, as evidenced by the reference to Flickr on the computer monitor.

Figure 22. **Generalist**. We show top three influential samples selected after the generalist stage.